9. Monzen, K., Hiroi, Y., Kudoh, S., Akazawa, H., Oka, T., Takimoto, E., Hayashi, D., Hosoda, T., Kawabata, M., Miyazono, K., Ishii, S., Yazaki, Y., Nagai, R., and Komuro, I. (2001) *J. Cell Biol.* **153,** 687–698
10. van Wijk, B., Moorman, A. F. M., and van den Hoff, M. J. B. (2007) *Cardiovasc. Res.* **74,** 244–255
11. Zhang, H., and Bradley, A. (1996) *Development* **122,** 2977–2986
12. Hogan, B. L. (1996) *Genes Dev.* **10,** 1580–1594
13. De Robertis, E. M., and Kuroda, H. (2004) *Annu. Rev. Cell Dev. Biol.* **20,** 285–308
14. Dosch, R., Gawantka, V., Delius, H., Blumenstock, C., and Niehrs, C. (1997) *Development* **124,** 2325–2334
15. Conley, C. A., Silburn, R., Singer, M. A., Ralston, A., Rohwer-Nutter, D., Olson, D. J., Gelbart, W., and Blair, S. S. (2000) *Development* **127,** 3947–3959
16. Coffinier, C., Ketpura, N., Tran, U., Geissert, D., and De Robertis, E. M. (2002) *Mech. Dev.* **119,** 179–184
17. Rentzsch, F., Zhang, J., Kramer, C., Sebald, W., and Hammerschmidt, M. (2006) *Development* **133,** 801–811
18. Ikeya, M., Kawada, M., Kiyonari, H., Sasai, N., Nakao, K., Furuta, Y., and Sasai, Y. (2006) *Development* **133,** 4463–4473
19. Moser, M., Binder, O., Wu, Y., Aitsebaomo, J., Ren, R., Bode, C., Bautch, V. L., Conlon, F. L., and Patterson, C. (2003) *Mol. Cell. Biol.* **23,** 5664–5679
20. Binnerts, M. E., Wen, X., Cante-Barrett, K., Bright, J., Chen, H. T., Asundi, V., Sattari, P., Tang, T., Boyle, B., Funk, W., and Rupp, F. (2004) *Biochem. Biophys. Res. Commun.* **315,** 272–280
21. Coles, E., Christiansen, J., Economou, A., Bronner-Fraser, M., and Wilkinson, D. G. (2004) *Development* **131,** 5309–5317
22. Kamimura, M., Matsumoto, K., Koshiba-Takeuchi, K., and Ogura, T. (2004) *Dev. Dyn.* **230,** 434–445
23. Rudnicki, M. A., and McBurney, M. W. (1987) in *Teratocarcinomas and Embryonic Stem Cells; A Practical Approach* (Robertson, E. J., ed) pp. 19–49, IRL Press, Oxford
24. Takahashi, T., Lord, B., Schulze, C. P., Fryer, R. M., Sarang, S. S., Gullans, S. R., and Lee, R. T. (2003) *Circulation* **107,** 1912–1916
25. Katagiri, T., Imada, M., Yanai, T., Suda, T., Takahashi, N., and Kamijo, R. (2002) *Genes Cells* **7,** 949–960
26. Tada, S., Era, T., Furusawa, C., Sakurai, H., Nishikawa, S., Kinoshita, M., Nakao, K., Chiba, T., and Nishikawa, S. (2005) *Development* **132,** 4363–4374
27. Naito, A. T., Akazawa, H., Takano, H., Minamino, T., Nagai, T., Aburatani, H., and Komuro, I. (2005) *Circ. Res.* **97,** 144–151
28. Stary, M., Pasteiner, W., Summer, A., Hrdina, A., Eger, A., and Weitzer, G. (2005) *Exp. Cell Res.* **310,** 331–343
29. Angello, J. C., Kaestner, S., Welikson, R. E., Buskin, J. N., and Hauschka, S. D. (2006) *Dev. Dyn.* **235,** 2122–2133
30. Wilkinson, D. G., Bhatt, S., and Herrmann, B. G. (1990) *Nature* **343,** 657–659
31. Parameswaran, M., and Tam, P. P. (1995) *Dev. Genet.* **17,** 16–28
32. Coucouvanis, E., and Martin, G. R. (1999) *Development* **126,** 535–546
33. Sater, A. K., and Jacobson, A. G. (1989) *Development* **105,** 821–830
34. Saga, Y., Hata, N., Kobayashi, S., Magnuson, T., Seldin, M. F., and Taketo, M. M. (1996) *Development* **122,** 2769–2778
35. Ying, Q. L., Nichols, J., Chambers, I., and Smith, A. (2003) *Cell* **115,** 281–292
36. Norton, J. D. (2000) *J. Cell Sci.* **113,** 3897–3905
37. Yuasa, S., Itabashi, Y., Koshimizu, U., Tanaka, T., Sugimura, K., Kinoshita, M., Hattori, F., Fukami, S., Shimazaki, T., Ogawa, S., Okano, H., and Fukuda, K. (2005) *Nat. Biotechnol.* **23,** 607–611
38. McMahon, J. A., Takada, S., Zimmerman, L. B., Fan, C. M., Harland, R. M., and McMahon, A. P. (1998) *Genes Dev.* **12,** 1438–1452
39. Miura, S., Davis, S., Klingensmith, J., and Mishina, Y. (2006) *Development* **133,** 3767–3775

MOLECULAR AND CELLULAR BIOLOGY, May 2008, p. 3424–3436 Vol. 28, No. 10
0270-7306/08/$08.00+0 doi:10.1128/MCB.02186-07

MURC, a Muscle-Restricted Coiled-Coil Protein That Modulates the Rho/ROCK Pathway, Induces Cardiac Dysfunction and Conduction Disturbance[▽]

Takehiro Ogata,[1] Tomomi Ueyama,[1]* Koji Isodono,[1,2] Masashi Tagawa,[1,2] Naofumi Takehara,[2] Tsuneaki Kawashima,[3] Koichiro Harada,[1] Tomosaburo Takahashi,[1,2] Tetsuo Shioi,[3] Hiroaki Matsubara,[1,2] and Hidemasa Oh[1]

Department of Experimental Therapeutics, Translational Research Center, Kyoto University Hospital, Kyoto 606-8507, Japan[1]; Department of Cardiovascular Medicine, Kyoto Prefectural University School of Medicine, Kyoto 602-8566, Japan[2]; and Department of Cardiovascular Medicine, Kyoto University Graduate School of Medicine, Kyoto 606-8507, Japan[3]

Received 11 December 2007/Returned for modification 10 January 2008/Accepted 4 March 2008

We identified a novel muscle-restricted putative coiled-coil protein, MURC, which is evolutionarily conserved from frog to human. MURC was localized to the cytoplasm with accumulation in the Z-line of the sarcomere in the murine adult heart. MURC mRNA expression in the heart increased during the developmental process from the embryonic stage to adulthood. In response to pressure overload, MURC mRNA expression increased in the hypertrophied heart. Using the yeast two-hybrid system, we identified the serum deprivation response (SDPR) protein, a phosphatidylserine-binding protein, as a MURC-binding protein. MURC induced activation of the RhoA/ROCK pathway, which modulated serum response factor-mediated atrial natriuretic peptide (ANP) expression and myofibrillar organization. SDPR augmented MURC-induced transactivation of the ANP promoter in cardiomyocytes, and RNA interference of SDPR attenuated the action of MURC on the ANP promoter. Transgenic mice expressing cardiac-specific MURC (Tg-MURC) exhibited cardiac contractile dysfunction and atrioventricular (AV) conduction disturbances with atrial chamber enlargement, reduced thickness of the ventricular wall, and interstitial fibrosis. Spontaneous episodes of atrial fibrillation and AV block were observed in Tg-MURC mice. These findings indicate that MURC modulates RhoA signaling and that MURC plays an important role in the development of cardiac dysfunction and conduction disturbance with increased vulnerability to atrial arrhythmias.

The heart is constantly exposed to biomechanical and neurohumoral stress, even under physiological conditions, and increased stress on the heart leads to hypertrophy and apoptosis of cardiomyocytes and ultimately heart failure (HF). Atrial fibrillation (AF) is one of the most common arrhythmias that produces substantially excess cardiovascular morbidity and mortality (13). Clinically, increased vulnerability to AF is associated with underlying heart disease, such as valvular heart disease, HF, coronary artery disease, and hypertension, particularly when left ventricular hypertrophy is present (13). The Z-disc in striated muscle constitutes an anchoring site for actin, titin, and nebulin filaments and plays a critical role in muscle structure and function, including sarcomeric assembly and organization, sarcolemmal membrane integrity, and muscle force generation and transmission (8). The Z-disc connects to the costamere, the basement membrane at periodic membrane-associated plaques, which serves to transmit force from the Z-disc to the sarcolemma and extracellular matrix (9). In addition to its role in muscle contraction, the Z-disc works as a biomechanical sensor that can respond to changes in tension in the sarcolemma. Various signaling molecules have been identified as components of the Z-disc, and a large number of the Z-disc-associated proteins have a dynamic distribution in muscle cells and shuttle between the Z-disc and other subcellular locations to transmit signals (8, 22, 35). Thus, the Z-disc is not only simply the structural border of the sarcomere but also functions in sensing and transmitting external and internal signals. Since the Z-disc is a multiprotein complex, the identification of the precise molecular mechanisms of the Z-disc and its role in signaling has become critical for understanding the regulation of cardiac function and the design of therapeutic strategies to prevent the progression to HF.

Rho GTPases are molecular switches that control a variety of signaling pathways in eukaryotic cells (10). The Rho family GTPase RhoA controls the formation of actin structures, and the RhoA-actin signaling pathway regulates serum response factor (SRF) transcriptional activity. SRF regulates serum-inducible and muscle-specific gene expression by binding to the serum response element (SRE) (also referred to as the CArG box). ROCK (Rho-kinase) is one of the downstream effectors of Rho GTPases (2, 32). In the heart, overexpression of RhoA resulted in sinus and atrioventricular (AV) nodal dysfunction, AF, and ventricular contractile failure with chamber enlargement and interstitial fibrosis (37). On the other hand, inhibition of Rho family protein activities by overexpression of Rho GDP dissociation inhibitor α resulted in an AV block with atrial enlargement and ventricular hypertrophy (47). These results suggest that fine-tuning of Rho GTPase signaling is required for maintaining cardiac rhythm, conduction, and structure.

* Corresponding author. Mailing address: Department of Experimental Therapeutics, Translational Research Center, Kyoto University Hospital, Kyoto 606-8507, Japan. Phone: 81-75-751-4763. Fax: 81-75-751-4741. E-mail: toueyama-circ@umin.ac.jp.

▽ Published ahead of print on 10 March 2008.

In this study, we sought to identify novel cardiac-restricted molecules that participate in cardiac homeostasis and pathogenesis. We identified MURC (*mu*scle-*r*estricted *c*oiled-coil protein) and characterized its function in cardiomyocytes and hearts.

MATERIALS AND METHODS

RNA extraction and quantitative reverse transcriptase (RT)-PCR. Total RNA was extracted from cells or tissues using an RNeasy Mini kit (Qiagen) or Trizol reagent (Invitrogen). Total RNA of human heart was purchased from Ambion. cDNA synthesis and kinetic real-time PCR were performed as described previously (33). Primers used were as follows: mouse MURC (mMURC) forward primer (5′-ACAGTCACACAGCAATACGGGCTA-3′) and mMURC reverse primer (5′-TTCTCGGGCAGGCTTCTGTCTTTA-3′); mouse atrial natriuretic peptide (ANP) forward primer (5′-AACCTGCTAGACCACCTGGA-3′) and mouse ANP reverse primer (5′-TGCTTTTCAAGAGGGCAGAT-3′); mouse brain natriuretic peptide (BNP) forward primer (5′-CTGAAGGTGCTGTCCC AGAT-3′) and mouse BNP reverse primer (5′-CCTTGGTCCTTCAAGAGCT G-3′); mouse serum deprivation response (mSDPR) forward primer (5′-ATGA GGAAGCCCTGGAAGAT-3′) and mSDPR reverse primer (5′-CCCAGATG ATGCTTTCTGGT-3′); mouse glyceraldehyde-3-phosphate dehydrogenase (GAPDH) forward primer (5′-TTGTGATGGGTGTGAACCACGAGA-3′) and mouse GAPDH reverse primer (5′-CATGAGCCCTTCCACAATGCCAA A-3′); mouse α-myosin heavy chain (αMHC) forward primer (5′-GAGGACCA GGCCAATGAGTA-3′) and mouse αMHC reverse primer (5′-GCTGGGTGT AGGAGAGCTTG-3′); mouse β-myosin heavy chain (βMHC) forward primer (5′-TCGATTTGGGAAATTCATCC-3′) and mouse βMHC reverse primer (5′-CGCATAATCGTAGGGGTTGT-3′); mouse sarcoplasmic reticulum Ca^{2+} ATPase 2 (SERCA2) forward primer (5′-CTGTGGAGACCCTTGGTTGT-3′) and mouse SERCA2 reverse primer (5′-CAGAGCACAGATGGTGGCTA-3′); mouse transforming growth factor β1 (TGF-β1) forward primer (5′-TTGCTTC AGCTCCACAGAGA-3′) and mouse TGF-β1 reverse primer (5′-TGGTTGTA GAGGGCAAGGAC-3′); mouse TGF-β2 forward primer (5′-CAGCGCTACA TCGATAGCAA-3′) and mouse TGF-β2 reverse primer (5′-CCTCGAGCTCT TCGCTTTTA-3′); mouse TGF-β3 forward primer (5′-GATGAGCACATAGC CAAGCA-3′) and mouse TGF-β3 reverse primer (5′-ATTGGGCTGAAAGG TGTGAC-3′); mouse procollagen type I α1 (Col1a1) forward primer (5′-GAG CGGAGAGTACTGGATCG-3′) and mouse Col1a1 reverse primer (5′-GCTT CTTTTCCTTGGGGTTC-3′); mouse Col1a2 forward primer (5′-CCGTGCTT CTCAGAACATCA-3′) and mouse Col1a2 reverse primer (5′-GAGCAGCCA TCGACTAGGAC-3′); mouse Col3a1 forward primer (5′-GTCCACGAGGTG ACAAAGGT-3′) and mouse Col3a1 reverse primer (5′-GATGCCCACTTGT TCCATCT-3′); rat MURC (rMURC) forward primer (5′-ACTGAAGATGAA GACCAGGACGCA-3′) and rMURC reverse primer (5′-TGTTAACAACGTA GCCCGTGTTGC-3′); rat ANP forward primer (5′-ATACAGTGCGGTGTCC AACA-3′) and rat ANP reverse primer (5′-CGAGAGCACCTCCATCTCTC-3′); rat BNP forward primer (5′-GGAAATGGCTCAGAGACAGC-3′) and rat BNP reverse primer (5′-CGATCCGGTCTATCTTCTGC-3′); and rat GAPDH forward primer (5′-ATGGGAAGCTGGTCATCAAC-3′) and rat GAPDH reverse primer (5′-GTGGTTCACACCCATCACAA-3′).

SAGE. Serial analysis of gene expression (SAGE) was performed as described previously (33). The SAGE libraries were constructed essentially following the I-SAGE long kit protocol (Invitrogen) using total RNA extracted from adult mouse hearts. Double-stranded cDNAs were digested with NlaIII, and the restriction enzyme was replaced by MmeI after linker ligation. Ditags produced from 400 PCRs were isolated, cleaved with NlaIII, and cloned into pZErO. All sequence files were processed using SAGE2000 version 4.5 software. The extracted tags were further processed to determine the identity of associated genes through several stringent filters using the CGAP website (http://cgap.nci.nih.gov/SAGE).

Plasmid constructs. The corresponding cDNA fragments for human MURC (hMURC), mMURC, and rMURC were cloned by PCR from human heart cDNA, mouse heart cDNA, and rat cardiomyocyte cDNA templates, respectively. PCR was performed using the following primers: hMURC forward primer (5′-ATGGAACATAATGGGTCTGC-3′) and hMURC reverse primer (5′-TTA CGATGAGTGCTTTAAATCTAAC-3′); mMURC forward primer (5′-ATGG AACACAACGGATCAGCT-3′) and mMURC reverse primer (5′-CTATTTG TAGTCTGAGGACTGCTTTAGCTCCA-3′); rMURC forward primer (5′-AT GGAACACAATGGATCTGC-3′) and rMURC reverse primer (5′-CTATGAG GACTGCTTTAATTCCAAC-3′). The cDNAs encoding mMURC and hMURC with a C-terminal Flag epitope were cloned into pcDNA3 (Invitrogen) to generate pcDNA3-mMURC and pcDNA3-hMURC, respectively. The corresponding cDNA fragment for human SDPR (hSDPR) was cloned by PCR from human heart cDNA template. PCR was performed using hSDPR forward primer (5′-A TGGGAGAGGACGCTGACAGGC-3′) and hSDPR reverse primer (5′-TCAC GGCAGTCTGATCCACAT-3′). The cDNA encoding hSDPR with a C-terminal hemagglutinin (HA) epitope was cloned into pcDNA3 to generate pcDNA3-hSDPR. The cDNA encoding hMURC was cloned into pGBKT7 (Clontech) to generate a bait vector, pGBKT7-hMURC. The RNA interference (RNAi) target sequences for rMURC (5′-TTCGAGTAACCAAAGTCGAAA-3′), rat SDPR (rSDPR, 5′-GAAGCAGTGTGTACAGGTGAA-3′), and green fluorescent protein (GFP; 5′-CGTAAACGCCCACAAGTTC-3′) were cloned into the BamHI-EcoRI sites of the RNAi-Ready-pSIREN-RetroQ vector (Clontech) as an inverted repeat with a hairpin loop spacer to generate RNAi-Ready-pSIREN-RetroQ-rMURC, RNAi-Ready-pSIREN-RetroQ-rSDPR, and RNAi-Ready-pSIREN-RetroQ-GFP (used as a control), respectively.

Northern blot analysis. Total RNA was isolated from tissues with Trizol reagent (Invitrogen). Total RNA was size fractionated by electrophoresis in a 1.3% agarose gel containing 2.2 M formaldehyde and transferred to nylon membranes. A HindIII fragment of pcDNA3-mMURC (nucleotides 1 to 797 of the mMURC open reading frame) was used as a probe.

Production of polyclonal antibody. Rabbit immunization was conducted by Medical & Biological Laboratories Co., Ltd. (Nagoya, Japan) using synthetic peptides spanning fragments of mMURC with N-terminal acetylation (GERLR QSGERFKKSISC). For immunostaining and Western blot analysis, immunoglobulin G (IgG) was purified from antisera with protein A-Sepharose beads.

Immunofluorescence microscopy. Specimens were fixed in 4% paraformaldehyde and stained with rabbit polyclonal anti-MURC antibody, mouse monoclonal anti-α-actinin antibody (Sigma), mouse monoclonal anti-α-smooth muscle actin antibody (Sigma), rat monoclonal anti-mouse CD31 antibody (BD Biosciences), rat monoclonal anti-HA antibody (Roche), mouse monoclonal anti-Flag antibody (Sigma), or rabbit polyclonal anti-Flag antibody (Sigma). Secondary antibodies were conjugated with Alexa Fluor 488, 555, or 594 (Invitrogen), and nuclei were visualized using 4′,6-diamino-2-phenylindole (DAPI; Invitrogen).

Cardiomyocyte culture. Rat neonatal cardiomyocytes, cultured from 1-day-old Sprague-Dawley rats, were prepared as described previously with slight modifications (42, 44). Briefly, ventricles were digested enzymatically, and cardiomyocytes were purified over a Percoll gradient. The culture medium was changed to serum-free medium after 24 h. Neonatal cardiomyocytes were cultured under serum-free conditions for 24 h before experiments. Adult cardiomyocytes were isolated from the hearts of male C57BL6 mice at 8 weeks of age. Ventricles were minced roughly and subsequently placed into 0.05% trypsin–EDTA (Invitrogen) at 4°C. After overnight incubation, ventricular tissue segments were put into Hanks' balanced salt solution buffer (Invitrogen) containing 0.1% (wt/vol) type 2 collagenase (Worthington Biochemical Corporation) at 37°C for 2 h. Dissociated adult cardiomyocytes were plated on 0.1% gelatin-coated slides and cultured in Dulbecco's modified Eagle's medium–F-12 medium with 5% bovine serum.

Aortic banding. Male mice were anesthetized with 2,2,2-tribromoethanol (0.25 mg/g of body weight; Aldrich). A midline abdominal incision was used to expose the suprarenal abdominal aorta. The aorta was tied with a 6-0 silk suture against a blunt needle (26 gauge). The needle was immediately removed, leaving the aortic lumen constricted to the diameter of the needle. Sham-operated mice were subjected to the same procedure without the aortic banding. Seven days after surgery, mice were sacrificed and total RNA was extracted from the heart.

Yeast two-hybrid screen. A *Saccharomyces cerevisiae* two-hybrid screen was performed using a Matchmaker Gal 4 two-hybrid system 3 (Clontech) and a Matchmaker pretransformed human heart cDNA library (Clontech) according to the manufacturer's instructions.

Replication-defective recombinant adenoviruses and gene transfer. The cDNAs encoding mMURC with a C-terminal Flag epitope and hSDPR with a C-terminal HA epitope were inserted into a pAxCAwtit cosmid vector in an adenovirus expression vector kit (Dual Version; Takara Bio Inc., Otsu, Japan). RNAi-Ready-pSIREN-RetroQ-rMURC and RNAi-Ready-pSIREN-RetroQ-luciferase (Clontech), which was used as a control, were digested with BglII and EcoRI to obtain the U6 promoter with each of the target sequences, and blunted fragments were inserted into a promoterless pAxcwit cosmid vector with an adenovirus expression vector kit (Dual Version). Recombinant adenoviruses expressing Flag-tagged mMURC (Ad-MURC), HA-tagged hSDPR (Ad-SDPR), LacZ (Ad-LacZ), MURC shRNA (Ad-rMURC shRNA), and Luc shRNA (Ad-Luc shRNA) were generated as described previously (43). Twenty-four hours after seeding, cardiomyocytes were infected with Ad-MURC, Ad-SDPR, Ad-LacZ, Ad-rMURC shRNA, or Ad-Luc shRNA diluted in the culture medium at a multiplicity of infection (MOI) of 10 or 20 and incubated at 37°C for 1 h. The

viral suspension was removed, and cardiomyocytes were cultured with serum-depleted culture medium. Phenylephrine (PE) or Y-27632 was added after infection.

Immunoprecipitation. COS cells were plated in 60-mm dishes. The following day, the cells were transfected with 1 μg of pcDNA3-hMURC and/or pcDNA3-hSDPR. The total plasmid amount was adjusted to 2.0 μg with an empty vector plasmid. Cardiomyocytes were plated in 60-mm dishes. The following day, the cells were infected with Ad-MURC and/or Ad-SDPR. The total MOI was adjusted to 20 with Ad-LacZ. Cells were cultured for another 48 h and lysed with a lysis buffer (20 mM HEPES, pH 7.7, 100 mM NaCl, 5 mM $MgCl_2$, 1% Nonidet P-40, 0.1 mM Na_3VO_4, 2 μg/ml aprotinin, 0.7 μg/ml pepstatin A, 0.1 mM phenylmethylsulfonyl fluoride, and 1 mM dithiothreitol). Cell lysates were incubated with anti-Flag M2 affinity gel (Sigma) or an anti-HA antibody and protein A-Sepharose beads (GE Healthcare) at 4°C. After the beads were extensively washed with the lysis buffer, the bound proteins were eluted by boiling the beads in sodium dodecyl sulfate (SDS) sample buffer and subjected to SDS-polyacrylamide gel electrophoresis (SDS-PAGE), followed by Western blot analysis.

Western blot analysis. Cell lysates were extracted with a lysis buffer containing 50 mM Tris-HCl (pH 7.4), 150 mM NaCl, 1 mM EDTA, 1% Nonidet P-40, 1 mM phenylmethylsulfonyl fluoride, 1× protease inhibitor cocktail (Pierce), 1 mM Na_3VO_4, and 1 mM NaF. Cell lysates were electrophoresed in 10% SDS-polyacrylamide gels and transferred to polyvinylidene difluoride membranes (Millipore). Membranes were subsequently incubated with primary antibodies against Flag (Sigma), HA, and MURC. Horseradish peroxidase–conjugated anti-rabbit IgG, anti-rat IgG, and anti-mouse IgG (GE Healthcare) were used as secondary antibodies.

RhoA activation assay. RhoA activity was determined from protein isolated from adenovirus-infected neonatal cardiomyocytes or heart tissues of transgenic mice using an absorbance-based G-LISA RhoA activation assay biochemistry kit (Cytoskeleton) according to the manufacturer's instructions. Cell protein was isolated on day 2 postinfection using the provided cell lysis buffer. Heart tissue protein of mice at 6 weeks of age was also isolated by homogenizing in cell lysis buffer. Cell or tissue lysates were clarified by centrifugation at 10,000 rpm at 4°C for 2 min, and these extracts were processed rapidly on ice and snap-frozen until the time of assay. Protein concentration was determined according to the manufacturer's protocol, and extracts were equalized to contain total protein concentrations of 1 mg/ml for the assay. Signals were measured at an absorbance of 490 nm using a microplate spectrometer as suggested by the manufacturer.

Transfection and reporter assay. COS cells were plated in six-well plates. The following day, the cells were transfected with 200 ng of ANP luciferase reporter construct (−638 ANP Luc; kindly provided by Kenneth R. Chien, Massachusetts General Hospital, Boston, MA) or no-SRE1/SRE2 mutant in the ANP luciferase reporter construct (kindly provided by Andrew Thorburn, Wake Forest University School of Medicine, NC). The cells were also transfected with 1.0 μg of expression vectors containing hMURC, mMURC, RhoA Val14, hSDPR, GFP shRNA, or rSDPR shRNA, 500 ng of a C3 expression vector, and 200 ng of pTKβ-Gal using FuGene6 reagent (Roche). The total plasmid amount was adjusted to 1.9 μg with an empty vector plasmid. An expression vector containing RhoA V14 (the mutant of Gly to Val at codon 14), which is a point-mutated active form of RhoA, was kindly provided by Yoshimi Takai (Osaka University, Suita, Japan). A C3 expression vector was kindly provided by Seigo Izumo (Novartis Institutes for Biomedical Research, Cambridge, MA). Cells were cultured for another 48 h, lysed with 200 μl of reporter lysis buffer (Promega), and assayed for luciferase activity (by using a Promega assay) and β-galactosidase activity. Luciferase activity was normalized against β-galactosidase activity.

Myofibrillar organization analysis. Ad-LacZ- or Ad-MURC-infected cardiomyocytes were incubated in serum-free medium. Y-27632 was added after infection. After 96 h of 10 μM Y-27632 treatment, cells were fixed in 4% paraformaldehyde and stained with fluorescein isothiocyanate-conjugated phalloidin (Sigma) for the detection of actin filaments. Ad-Luc shRNA- or Ad-rMURC shRNA-infected cardiomyocytes were incubated in serum-free medium at 37°C for 48 h prior to stimulation with 100 μM PE. After 48 h of PE stimulation, cells were fixed and stained with fluorescein isothiocyanate-conjugated phalloidin.

Generation of transgenic mice. The cDNA encoding Flag-tagged mMURC was cloned into the third 5′-untranslated exon of αMHC promoter plasmid clone 26 (a generous gift from Jeffrey Robbins, Cincinnati Children's Hospital Medical Center, Cincinnati, OH) (16), and transgenic mice were generated as described previously (25). All of the aspects of animal care and experimentation performed in this study were approved by the Institutional Animal Care and Use Committee of Kyoto University.

Echocardiography and electrophysiological analysis. Echocardiographic examination of mice was performed as described previously (25, 26, 39). Briefly, mice were anesthetized with 2,2,2-tribromoethanol (0.20 mg/g), and M-mode recordings of the left ventricle (LV) were obtained at the level of the papillary muscles from a parasternal window using a Hewlett-Packard (Andover) Sonos 5500 equipped with a 12-MHz probe. Mice anesthetized with 2,2,2-tribromoethanol (0.20 mg/g) by intraperitoneal injection were analyzed by multilead-surface electrocardiogram (ECG). ECG recordings were performed using an ECG-9902 (Nihon Kohden, Tokyo, Japan).

Hemodynamic measurements. For left ventricular catheterization with a 1.0-F high-fidelity micromanometer-tipped catheter (model SPR-1000; Millar Instruments), mice were anesthetized with 2,2,2-tribromoethanol (0.25 mg/g), subsequently anesthetized with isoflurane (2.5% [vol/vol] in O_2), and placed on a 36.5° table. A microtip catheter was inserted into the LV via the right carotid artery. To determine cardiac contractile and diastolic function, signals for LV pressure and the maximal rates of systolic pressure increase (maximum dP/dt) and isovolumetric relaxation (minimum dP/dt) were recorded at 1,000 Hz and analyzed by using a PowerLab system (AD Instruments).

Microarray analysis. Total RNA isolated from LV tissue was extracted using an RNeasy Mini kit and treated with the DNase I (Qiagen) according to the manufacturer's instructions. DNA microarrays used in these experiments were produced using the Mouse Genome Oligo 4.0 set of 70-mer oligonucleotides (Operon). Hybridization, processing, and the scanning process were done by Filgen Incorporated (Nagoya, Japan). Scan data images were analyzed using Microarray Data Analysis Tool version 2.0 software (Filgen).

Statistical analysis. All experiments were performed at least three times. Data are expressed as means ± standard errors and were analyzed by one-way analysis of variance with post hoc analysis. A P value of <0.05 was considered significant.

RESULTS

Cloning of MURC. To identify unknown cardiac-specific genes, we performed SAGE (45) using RNA isolated from the hearts of adult mice and searched expressed sequence tag databases for novel sequences found only in cardiac cDNA libraries. Sequences that did not correspond to known genes were then used as probes for Northern blot analysis of adult mouse tissues, in order to confirm their cardiac-specific expression. One of the cDNAs identified in this screen appeared to be a muscle-restricted gene, and the extended cDNA sequence encoded a novel protein of 362 amino acids (Fig. 1). We then isolated human and rat orthologues of this gene by using human heart and rat cardiomyocyte cDNAs. Northern blot analysis of RNA from adult mouse tissues revealed abundant expression of this transcript in the heart and skeletal muscle (Fig. 2A). Weaker signals were found in the aorta and lung, suggesting expression of this transcript in vascular smooth muscle cells. We refer to this gene as MURC (*mu*scle-*r*estricted *c*oiled-coil protein), because the predicted open reading frame of MURC contains a putative coiled-coil motif. Database searches revealed that hMURC is encoded by a gene located on human chromosome 9q31. A cDNA encoding a MURC-like protein was also identified in the *Xenopus laevis* expressed sequence tag database (accession number NM_001097894). These findings suggest that MURC is an evolutionarily conserved protein in vertebrates.

Subcellular localization of MURC in cardiomyocytes. To identify a cell source expressing MURC in the heart, we separated cardiomyocytes from noncardiomyocytes using a rat primary culture and performed real-time RT-PCR. As shown in Fig. 2B, the MURC transcript was found to be much more abundant in cardiomyocytes than in noncardiomyocytes, indicating that the major source of MURC in the heart is cardiomyocytes. We then performed immunostaining of adult mouse heart sections with an anti-MURC antibody to investigate the subcellular localization of MURC in cardiomyocytes. MURC staining was detected in the cytoplasm with a striated and

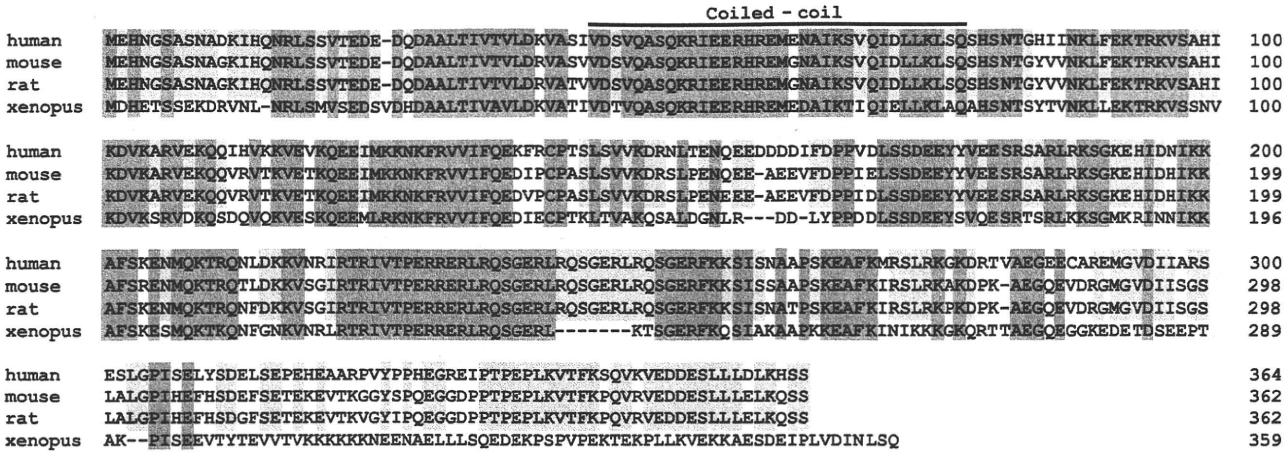

FIG. 1. Primary sequence of MURC. Alignment and amino acid sequence comparison of human MURC (GenBank accession number EU487253), mouse MURC (EU487254), and rat MURC (EU487255) and homology with a sequence from *Xenopus* (NM_001097894). Identical amino acids are shaded in gray, and gaps are represented by a dash. Positions in the amino acid sequence are given by the numbers. MURC contains a predicted coiled-coil domain.

periodic staining pattern and was partly colocalized with α-actinin in the Z-line (Fig. 3A), suggesting that MURC interacts with the Z-disc. Besides cardiomyocytes, MURC staining was also detected in vascular smooth muscle cells with a lower intensity than in cardiomyocytes, but not in other surrounding cells, including vascular endothelial cells (Fig. 3B and C), confirming the muscle-specific expression. In vascular smooth muscle cells, MURC staining was detected diffusely in the cytoplasm.

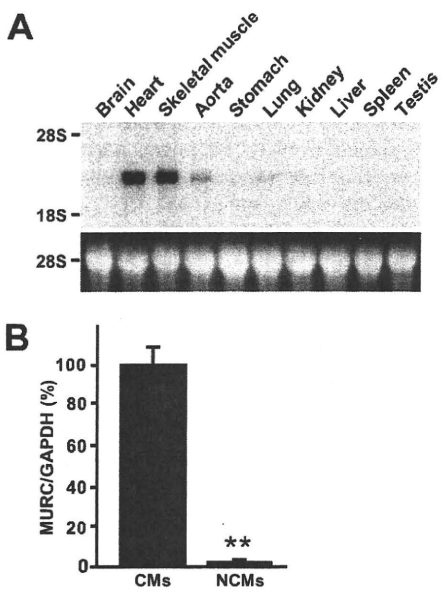

FIG. 2. MURC expression in tissues. (A) Blots were made with total RNA (20 μg) isolated from tissues of adult mice. The MURC transcript was observed in heart, skeletal muscle, aorta, and lung. 28S RNA was used as a control for assessing RNA loading. (B) Real-time RT-PCR was performed with cDNAs from cultured rat neonatal cardiomyocytes (CMs) and noncardiomyocytes (NCMs). **, $P < 0.01$ compared with CMs.

MURC expression in hearts under physiological and pathological conditions. To evaluate whether MURC expression is regulated during heart development, we analyzed mRNA expression in hearts of embryo, neonate, and adult mice. MURC mRNA expression in the heart was detected at embryonic day 10.5 (E10.5) (Fig. 4A, left). Real-time RT-PCR with RNA isolated from embryo (E10.5, E13. 5, E15.5, and E17.5), neonate, and adult hearts revealed that MURC mRNA expression increased during the developmental process from the embryonic stage to adulthood (Fig. 4A, right). We then investigated whether MURC expression might be regulated under pathological conditions in the postnatal heart. We performed abdominal aortic banding to make hypertrophied hearts in mice. Seven days after abdominal aortic constriction, the heart weight normalized to body weight ratio (HW/BW ratio) (band, 4.47 ± 0.03; sham, 4.09 ± 0.04; $P < 0.01$) and the heart weight normalized to tibial length ratio (HW/TL ratio) (band, 5.90 ± 0.06; sham, 5.21 ± 0.07; $P < 0.01$) were increased in banded mice compared with sham-operated mice, indicating that cardiac hypertrophy had indeed developed in the banded mice. As shown in Fig. 4B, MURC mRNA expression significantly increased in hypertrophied hearts (2.27-fold ± 0.12-fold; $P <$ 0.01 compared with sham-operated mice).

Identification of SDPR as a MURC-binding protein. To elucidate the molecular mechanism involving MURC, we screened over 5×10^7 clones of a human heart cDNA library with hMURC as the "bait" using the yeast two-hybrid system. In this screen, we obtained 13 independent clones. Sequence analysis showed that five isolated cDNAs encoded copper metabolism domain containing 1 (COMMD1) and two isolated cDNAs encoded leucine zipper protein 1 (LUZP1). COMMD1 and LUZP1 were excluded during verification of the protein interaction. The eight other isolated cDNAs encoded SDPR, which is a phosphatidylserine (PS)-binding protein (5, 17, 18, 30). An amino acid homology search revealed that hSDPR was 31% identical to hMURC. A database search for conserved domains revealed that hSDPR also has a predicted coiled-coil

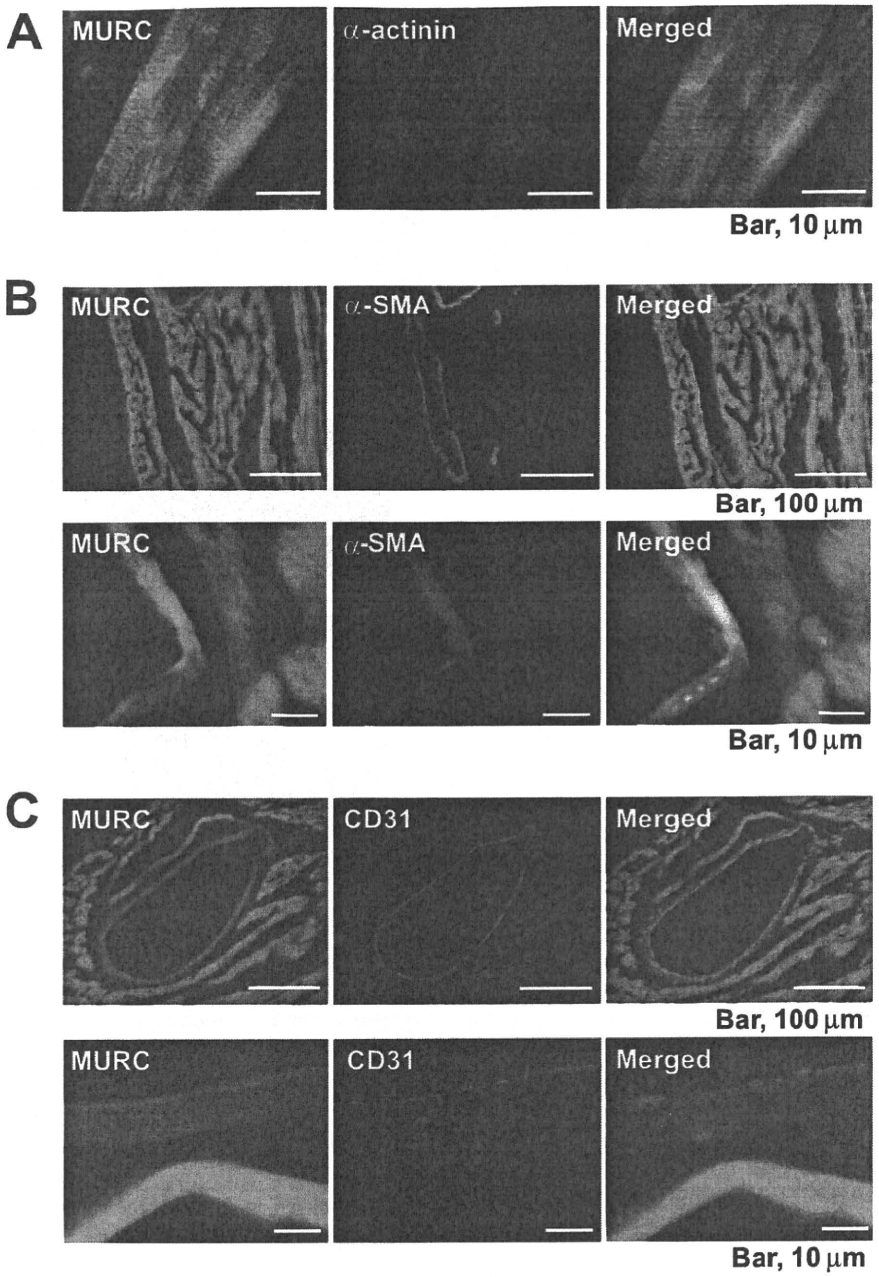

FIG. 3. Localization of MURC in the heart. (A) Immunostaining was performed using adult mouse heart sections with anti-MURC and anti-α-actinin antibodies. (B and C) Immunostaining was performed using adult mouse heart sections with an anti-MURC antibody and an anti-α-smooth muscle actin (SMA) antibody (upper panels) or an anti-CD31 antibody (lower panels). Nuclei were stained by DAPI (blue). Higher-magnification images are shown in lower panels.

domain. To examine the association between MURC and SDPR in mammalian cells, we transfected COS cells with constructs encoding Flag-tagged hMURC and HA-tagged hSDPR. Western blot analysis showed that hMURC was coimmunoprecipitated with hSDPR (Fig. 5A). Furthermore, we performed immunoprecipitation using cardiomyocytes infected with Ad-MURC and/or Ad-SDPR. As shown in Fig. 5B, Flag-tagged MURC was coimmunoprecipitated with HA-tagged SDPR in cardiomyocytes, confirming the interaction of MURC with SDPR in cardiomyocytes. In human and mouse tissues, SDPR mRNA has been shown to be highly expressed in heart and lung (17, 18). To assess the subcellular localization of SDPR, isolated adult cardiomyocytes were infected with Ad-SDPR. As shown in Fig. 5C, exogenous HA-tagged SDPR was localized to the cytoplasm, and MURC was localized to the cytoplasm and the Z-line. We then examined SDPR mRNA expression during heart development. As shown in Fig. 5D, SDPR mRNA expression in hearts gradually increased during embryonic stages and reached a maximum in neonates. Furthermore, SDPR mRNA expression increased significantly in

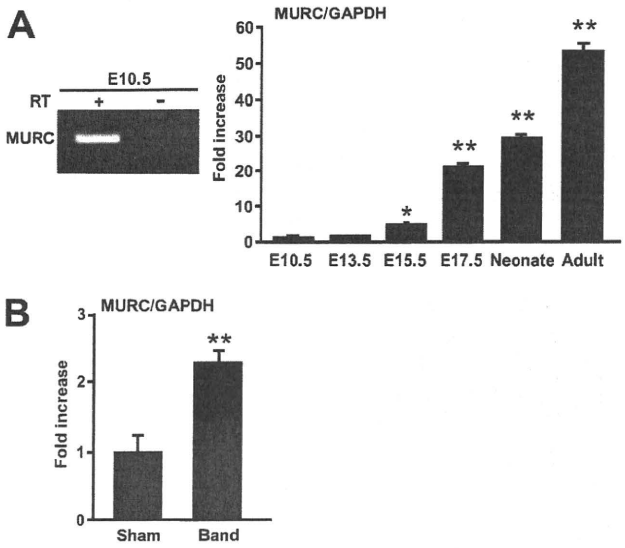

FIG. 4. MURC expression in the heart. (A) RT-PCR was performed with cDNAs from hearts at E10.5 (left). Real-time RT-PCR was performed with cDNAs from embryonic (E10.5, E13.5, E15.5, and E17.5), neonatal, and adult hearts (right). *, $P < 0.05$ compared with E10.5; **, $P < 0.01$ compared with E10.5. (B) Real-time RT-PCR was performed with cDNAs from hearts of sham-operated mice (sham) and abdominal aortic-banded mice (band). Seven days after surgery, total RNA was isolated from hearts. **, $P < 0.01$ compared with sham.

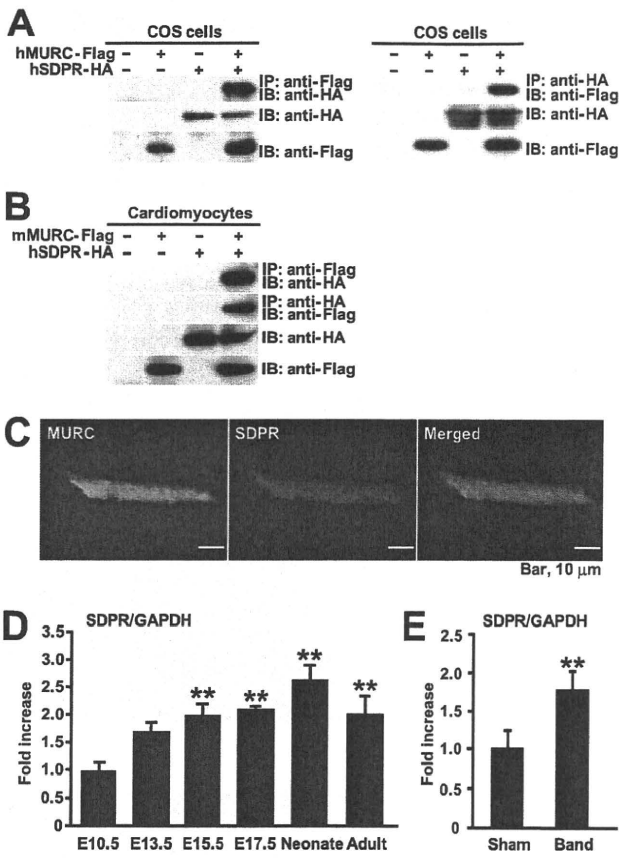

FIG. 5. Identification of SDPR as a MURC-binding protein and SDPR expression in the heart. (A) Immunoprecipitation from COS cells expressing hMURC-Flag and/or hSDPR-HA. hMURC-Flag alone, hSDPR-HA alone, or both proteins were transiently expressed in COS cells. Each cell extract was subjected to immunoprecipitation with the anti-Flag or anti-HA monoclonal antibody. The immunoprecipitate was then subjected to SDS-PAGE, followed by Western blot analysis with the anti-Flag or anti-HA monoclonal antibody. IP, immunoprecipitation; IB, immunoblot assay. (B) Immunoprecipitation from cardiomyocytes infected with Ad-MURC and/or Ad-SDPR. LacZ, mMURC-Flag with LacZ, hSDPR-HA with LacZ, or mMURC-Flag with hSDPR-HA was transiently expressed in cardiomyocytes. Each cell extract was subjected to immunoprecipitation with the anti-Flag or anti-HA monoclonal antibody. The immunoprecipitate was then subjected to SDS-PAGE, followed by Western blot analysis with the anti-Flag or anti-HA monoclonal antibody. (C) Localization of SDPR in adult cardiomyocytes. Adult cardiomyocytes were infected with Ad-SDPR at an MOI of 10. Immunostaining was performed using isolated adult mouse cardiomyocytes with anti-MURC and anti-HA antibodies. Nuclei were stained by DAPI (blue). (D) Real-time RT-PCR was performed with cDNAs from embryonic (E10.5, E13.5, E15.5, and E17.5), neonatal, and adult hearts. **, $P < 0.01$ compared with E10.5. (E) Real-time RT-PCR was performed with cDNAs from hearts of sham-operated mice and abdominal aortic-banded mice. Seven days after surgery, total RNA was isolated from hearts. **, $P < 0.01$ compared with sham.

hypertrophied hearts (Fig. 5E) (1.78-fold ± 0.14-fold; $P < 0.01$ compared with sham-operated mice).

MURC activates RhoA and induces ANP mRNA expression and myofibrillar organization through the Rho/ROCK signaling pathway. SDPR is a PS-binding protein (5, 17, 18, 30). PS is implicated in signaling pathways, and PS-binding proteins contribute to a wide range of cellular process (40). Among PS-binding proteins, conventional protein kinase C (PKC) and Raf-1 have been reported to be implicated in the development of cardiac hypertrophy and heart failure (7, 31, 40). The observation of the interaction of MURC with SDPR prompted us to investigate the effect of MURC on signaling pathways in cardiomyocytes. The ANP gene is well-suited for this purpose, as it has been used as a molecular marker to explore signaling pathways that regulate cardiac gene expression during development and disease, and reactivation of ANP expression is part of a conserved adaptive change in molecular phenotypes in response to heart failure (24). Overexpression of MURC in cardiomyocytes using Ad-MURC induced ANP mRNA expression (Fig. 6A). ANP mRNA expression in cardiomyocytes is known to be regulated by the Rho/ROCK pathway (23). Furthermore, the cardiac phenotype of transgenic mice expressing Flag-tagged MURC (Tg-MURC), as described below, was reminiscent of that of transgenic mice expressing RhoA (37). Therefore, we examined whether MURC might alter RhoA activity in cardiomyocytes. RhoA was significantly activated by MURC in cardiomyocytes (Fig. 6B) (1.41-fold ± 0.07-fold; $P < 0.05$ compared with Ad-LacZ-infected cardiomyocytes). MURC-induced ANP mRNA expression was attenuated by a ROCK inhibitor, Y-27632, in a dose-dependent manner (Fig. 6C).

To further examine the effect of MURC signaling on the transcription of ANP, we performed a luciferase reporter assay using the ANP promoter (−638 ANP Luc), which has two SRF-binding sites (21). hMURC transactivated −638 ANP Luc, and the extent of activation by mMURC was similar to that caused by hMURC (Fig. 6D). As shown in Fig. 6E, an activated mutant of RhoA, RhoA V14, transactivated −638

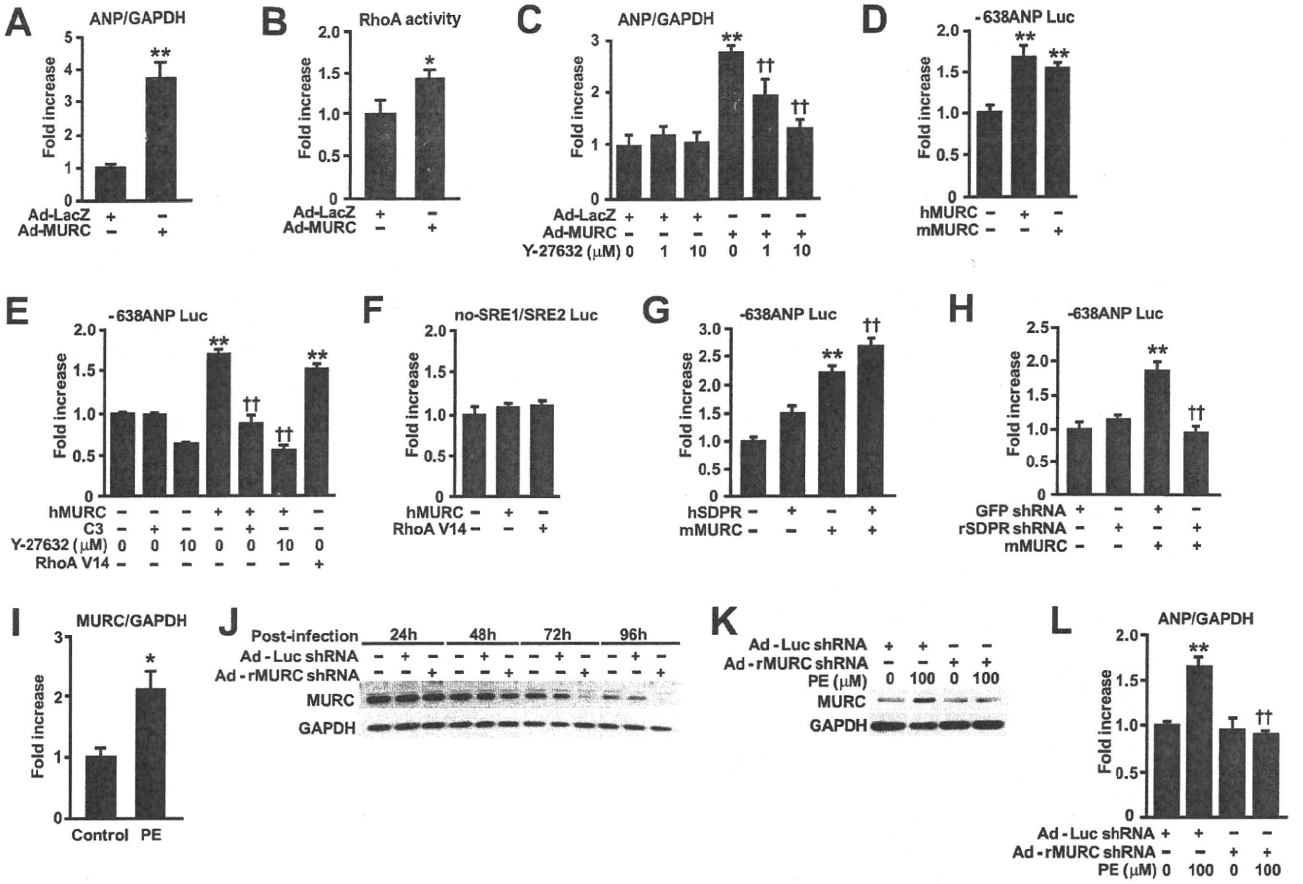

FIG. 6. Induction of ANP expression by MURC through the Rho/ROCK signaling pathway. (A and C) The bar graph shows real-time RT-PCR analysis of ANP mRNA expression in rat neonatal cardiomyocytes. Cells were infected with Ad-LacZ or Ad-MURC at an MOI of 10 and then harvested 48 h after the infection. Y-27632 was added after infection. **, $P < 0.01$ compared with Ad-LacZ; ††, $P < 0.01$ compared with Y-27632-treated Ad-LacZ. (B) The bar graph shows RhoA activity in rat neonatal cardiomyocytes. Cells were infected with Ad-LacZ or Ad-MURC at an MOI of 10 and then harvested 48 h after infection. *, $P < 0.05$ compared with Ad-LacZ. (D to F) The bar graphs show a reporter assay using −638 ANP Luc or no-SRE1/SRE2 Luc. hMURC, mMURC, C3, and/or RhoA V14 were cotransfected with −638 ANP Luc or no-SRE1/SRE2 Luc in COS cells. Cells were pretreated with Y-27632 for 30 min before transfection. Cells were harvested 48 h after transfection. **, $P < 0.01$ compared with control; ††, $P < 0.01$ compared with hMURC. (G and H) The bar graphs show a reporter assay using −638 ANP Luc. mMURC, hSDPR, GFP-shRNA, and/or rSDPR-shRNA was cotransfected with −638 ANP Luc in rat neonatal cardiomyocytes. Cells were harvested 48 h after transfection. **, $P < 0.01$ compared with control; ††, $P < 0.01$ compared with mMURC. (I) The bar graph shows real-time RT-PCR analysis of endogenous MURC mRNA expression. Rat neonatal cardiomyocytes were treated with vehicle or PE (100 μM) for 48 h and then harvested. *, $P < 0.05$ compared with vehicle. (J and K) The endogenous MURC protein level in neonatal cardiomyocytes was assessed by Western blot analysis. Cells were infected with or without Ad-Luc shRNA or Ad-rMURC shRNA at an MOI of 20. Cardiomyocytes treated with vehicle or PE were incubated for 48 h and then harvested. (L) The bar graph shows real-time RT-PCR analysis of ANP mRNA expression in neonatal cardiomyocytes. Cells were infected with Ad-Luc shRNA or Ad-rMURC shRNA at an MOI of 20. After 72 h of incubation, cells were treated with PE for another 24 h. **, $P < 0.01$ compared with Ad-Luc shRNA; ††, $P < 0.01$ compared with PE-treated Ad-LacZ shRNA.

ANP Luc. When Rho signaling was inhibited by C3, which specifically ADP-ribosylates Rho and inhibits its function (3), or Y-27632, MURC-induced transactivation of −638 ANP Luc was attenuated. We examined the requirement for the SRE sites in the ANP promoter for responsiveness to MURC signaling using no-SRE1/SRE2 Luc, which has mutations in both SREs in −638 ANP Luc (21, 41). As RhoA signaling has been reported to regulate SRF transcriptional activity (6, 14, 20, 44), the action of RhoA V14 was abolished in no-SRE1/SRE2 Luc, and the action of MURC was also abolished in no-SRE1/SRE2 Luc (Fig. 6F).

We then examined the role of SDPR in the MURC action in cardiomyocytes. When SDPR was transfected with MURC, SDPR augmented MURC-induced transactivation of −638 ANP Luc (Fig. 6G). RNAi using rSDPR shRNA was performed in neonatal rat cardiomyocytes to determine whether SDPR was required for the action of MURC. To evaluate the effect of rSDPR RNAi, we transfected COS cells with plasmids encoding Flag-tagged rSDPR and rSDPR shRNA. The protein expression of Flag-tagged rSDPR was inhibited by rSDPR RNAi (data not shown). rSDPR RNAi attenuated MURC-induced transactivation of −638 ANP Luc in cardiomyocytes (Fig. 6H). To exclude off-target effects of the rSDPR shRNA used, we used another shRNA sequence targeting SDPR and obtained similar effects on −638 ANP Luc (data not shown).

PE, an α1-adrenergic receptor agonist, induced MURC

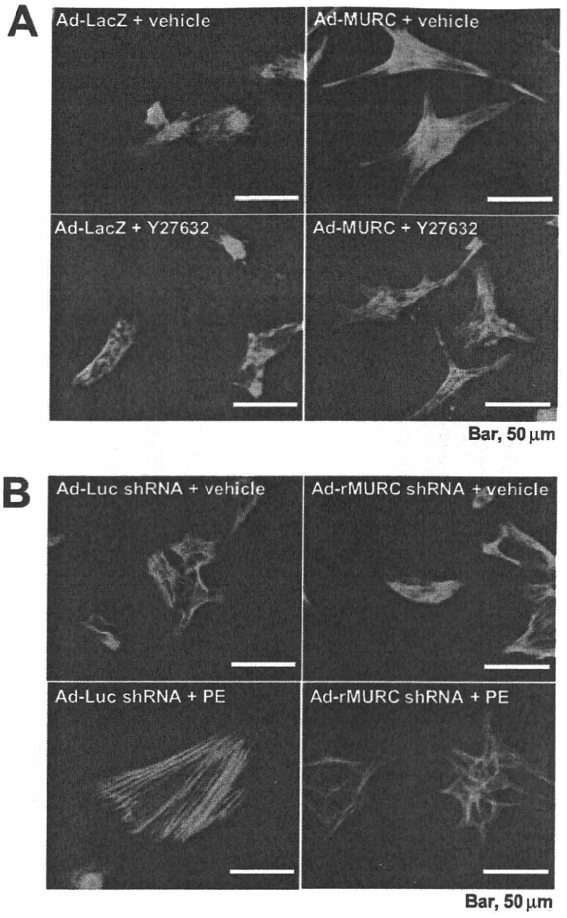

FIG. 7. Induction of myofibrillar organization by MURC through the Rho/ROCK signaling pathway. (A) Cardiomyocytes were infected with Ad-LacZ or Ad-MURC at an MOI of 10. After infection, cells were treated with vehicle or 10 μM Y-27632. Ninety-six hours later, cells were stained with fluorescein isothiocyanate-conjugated phalloidin. (B) Cardiomyocytes were infected with Ad-Luc shRNA or Ad-rMURC shRNA at an MOI of 20. After 48 h of serum deprivation, cells were treated with vehicle or 100 μM PE. Forty-eight hours later, cells were stained with phalloidin.

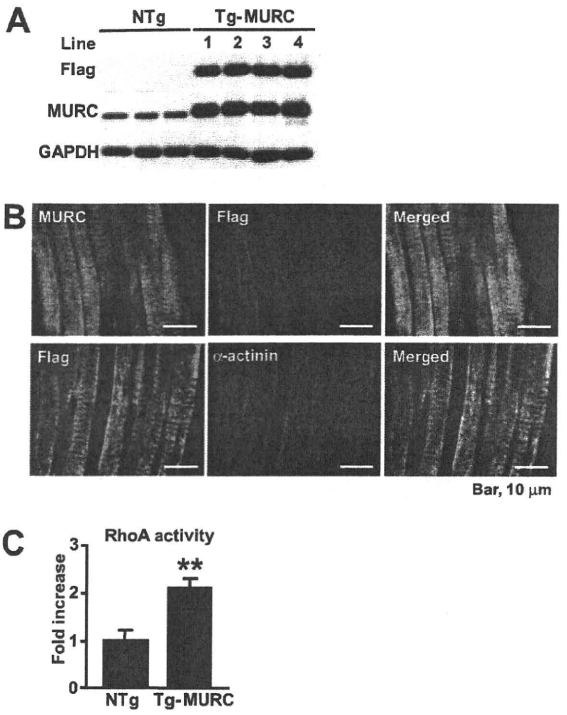

FIG. 8. Generation of a transgenic mouse expressing MURC. (A) Expression level of MURC protein in the heart. Heart lysates from NTg and Tg-MURC mice (line 1 to 4) were immunoblotted with antibodies against Flag (top panel), MURC (middle panel), or GAPDH as an internal control (bottom panel). (B) Subcellular localization of Flag-tagged MURC in cardiomyocytes of Tg-MURC mice. Immunostaining was also performed using adult mouse heart sections with an anti-Flag antibody, an anti-MURC antibody (upper panels), or an anti-α-actinin antibody (lower panels). (C) The bar graph shows RhoA activity in the hearts of NTg and Tg-MURC mice. **, $P < 0.01$ compared with NTg mice.

mRNA expression in cardiomyocytes (Fig. 6I). To directly examine the biological effects of MURC, we made a recombinant adenovirus expressing rMURC shRNA (Ad-rMURC shRNA) and examined the effect of MURC on PE-induced ANP mRNA expression. MURC protein expression was repressed in a time-dependent manner in cardiomyocytes infected with Ad-rMURC shRNA (Fig. 6J). When PE-induced upregulation of MURC protein was inhibited by Ad-MURC shRNA (Fig. 6K), PE-induced ANP mRNA expression was attenuated (Fig. 6L). We used another shRNA sequence targeting MURC and obtained a similar effect on −638 ANP Luc (data not shown).

The Rho/ROCK pathway has been also shown to mediate myofibrillar organization in cardiomyocytes (23). Therefore, we examined whether MURC could affect myofibrillar organization. Overexpression of MURC in cardiomyocytes using Ad-MURC induced myofibrillar organization, and MURC-induced myofibrillar organization was inhibited by Y-27632 (Fig. 7A). Furthermore, PE-induced myofibrillar organization was attenuated in cardiomyocytes infected with Ad-rMURC shRNA (Fig. 7B). Thus, MURC also affected myofibrillar organization in cardiomyocytes.

Generation of transgenic mice expressing MURC. To assess the functional effect of MURC in postnatal hearts, cardiac-specific transgenic mice expressing Flag-tagged MURC, Tg-MURC mice, were generated under the control of the αMHC promoter (16). Western blot analysis using an anti-Flag antibody and an anti-MURC antibody revealed that four independent lines of transgenic mice expressed comparable levels of transgenic protein (Fig. 8A). Immunostaining showed that Flag-tagged MURC was localized to the cytoplasm and the Z-line in cardiomyocytes of Tg-MURC mice (Fig. 8B). This finding supports the subcellular localization of MURC in cardiomyocytes, which was shown in Fig. 3A. We examined RhoA activity in the hearts of Tg-MURC mice. Consistent with the in vitro data, RhoA activity increased significantly in the hearts of Tg-MURC mice at 13 weeks of age (Fig. 8C) (2.11-fold ± 0.12-fold; $P < 0.01$ compared with nontransgenic [NTg] mice).

Cardiac contractile dysfunction in Tg-MURC mice. We measured heart weight at 13 weeks of age in Tg-MURC mice (Table 1). Although the HW/BW ratio in Tg-MURC mice was significantly lower than that in NTg mice, no significant differ-

TABLE 1. Morphometric analysis of NTg and Tg-MURC mice[a]

Mice (*n*)	BW (g)	TL (mm)	HW (mg)	HW/BW (mg/g)	HW/TL (mg/mm)	LW (mg)	LW/BW (mg/g)	LW/TL (mg/mm)
NTg (4)	25.00 ± 0.20	17.30 ± 0.12	120.50 ± 3.88	4.82 ± 0.19	6.97 ± 0.27	137.75 ± 2.63	5.51 ± 0.09	7.96 ± 0.16
Tg-MURC (6)	26.33 ± 0.65	17.58 ± 0.14	113.67 ± 4.74	4.31 ± 0.11*[b]	6.47 ± 0.26	140.67 ± 3.18	5.35 ± 0.14	8.00 ± 0.17

[a] BW, body weight; TL, tibial length; HW, heart weight; LW, lung weight. Values are expressed as means ± standard errors.
[b] *, $P < 0.05$ compared with sex-matched NTg mice.

ence in the HW/TL ratio was observed between Tg-MURC and NTg mice. The hearts of Tg-MURC mice at 13 weeks of age showed atrial chamber enlargement with a reduction in ventricular wall thickness (Fig. 9A and B). Histological assessment of cardiac pathology demonstrated a large organized thrombus in the left atrium (Fig. 9B). Diffuse interstitial fibrosis was detected in both atria and ventricles of Tg-MURC mice (Fig. 9C and D).

To address the functional consequences of MURC expression in vivo, echocardiography was performed on 12-week-old Tg-MURC and NTg mice, which confirmed reduced posterior wall thickness and depressed left ventricular systolic function in Tg-MURC mice compared with NTg mice (Table 2). Furthermore, we assessed systolic and diastolic LV pressures, contractility, and relaxation in Tg-MURC mice at 13 weeks of age. In Tg-MURC mice, the maximum LV *dP/dt* was significantly lower compared with that in NTg mice (Table 3). Thus, Tg-MURC mice showed cardiac contractile dysfunction associated with cardiac fibrosis.

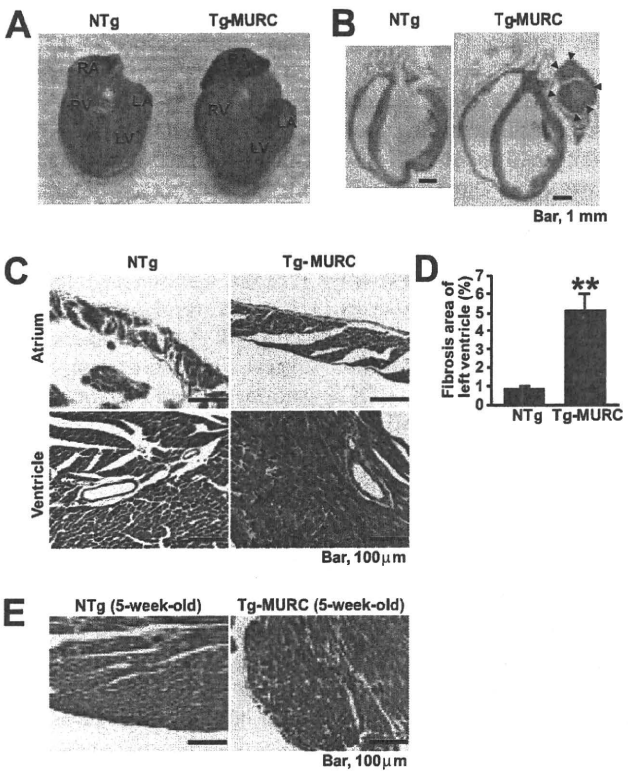

FIG. 9. Characterization of cardiac phenotypes in a transgenic mouse expressing MURC. (A) Representative hearts from 13-week-old NTg (left) and Tg-MURC (right) mice. (B) Sagittal sections of hearts from 13-week-old NTg (left panel) and Tg-MURC (right panel) mice. Arrows indicate a thrombus in the left atrium. RA, right atrium; LA, left atrium; RV, right ventricle; LV, left ventricle. (C) Histological assessment of cardiac fibrosis by Masson's trichrome staining. Representative trichrome-stained sections of cardiac atria (upper panels) and ventricles (lower panels) in 13-week-old NTg (left) and Tg-MURC (right) mice. (D) Quantification of fibrosis area (blue) from trichrome-stained cardiac histological sections in 13-week-old NTg versus Tg-MURC mice. **, $P < 0.01$ compared with NTg mice. (E) Histological assessment of the size of cardiomyocytes. Representative Masson's trichrome-stained sections of cardiac ventricles in NTg (left) and Tg-MURC (right) mice at 5 weeks of age.

We then examined the heart sections of Tg-MURC mice at 5 weeks of age to determine the earlier responses of cardiomyocytes to the MURC action in vivo. As shown in Fig. 9E, the cross-sectional area of cardiomyocytes in Tg-MURC mice was bigger than that in NTg mice (1.46-fold ± 0.02-fold; $P < 0.01$ compared with NTg mice), and various sizes of cardiomyocytes were observed in Tg-MURC mice. These findings suggest that the cardiac dysfunction in 12-week-old Tg-MURC mice is likely to be the end point of a pathological hypertrophy.

Conduction disturbances and increased vulnerability to atrial arrhythmias in Tg-MURC mice. ECGs were obtained from NTg and Tg-MURC mice at 9 and 12 weeks of age. Among 12 Tg-MURC mice analyzed by ECG at 9 weeks of age, 2 Tg-MURC mice (numbers 436 and 443) showed AF, 1 Tg-MURC mouse (429) showed complete AV block, and the other Tg-MURC mice showed AV conduction defects evidenced by prolongation of the PR interval (Fig. 10A). At 12 weeks of age, in Tg-MURC mouse 436 AF was sustained, whereas in Tg-MURC mouse 429 it showed a shift from complete AV block to AF, and Tg-MURC mouse 443 showed a shift from AF to complete AV block. The ECGs of other Tg-MURC mice with sinus rhythm (e.g., number 400) at 12 weeks of age demonstrated slow heart rate and prolongation of the PR interval (Fig. 10B). Furthermore, 16 Tg-MURC mice showed cardiac arrhythmias, including AF and AV block, among 38 Tg-MURC mice up to 20 weeks of age, whereas among 51 NTg mice, no mice showed cardiac arrhythmia.

To identify a molecular signature for the susceptibility to heart failure and atrial arrhythmias conferred by MURC, we compared microarray expression profiles of the ventricular myocardium from Tg-MURC and NTg mice and verified the findings by real-time PCR. ANP, BNP, βMHC, and fibrosis-related genes, such as TGF-β1, TGF-β2, TGF-β3, and procollagens, were upregulated in Tg-MURC mice compared with NTg mice, whereas SERCA2 was downregulated in Tg-MURC mice compared with NTg mice (Table 4).

To examine the role of MURC in ANP expression in vivo, we compared ANP mRNA expression in embryonic (E10.5), neonatal, and adult hearts of NTg and Tg-MURC mice by real-time RT-PCR. As shown in Fig. 11, ANP mRNA expres-

TABLE 2. Echocardiographic analysis of NTg and Tg-MURC mice[a]

Mice (n)	LVDd (mm)	LVDs (mm)	IVST (mm)	PWT (mm)	FS (%)
NTg (9)	3.27 ± 0.06	1.62 ± 0.05	0.58 ± 0.03	0.71 ± 0.03	50.6 ± 0.81
Tg-MURC (9)[b]	3.92 ± 0.13**	2.60 ± 0.14**	0.55 ± 0.02	0.58 ± 0.03**	34.2 ± 1.72**

[a] LVDd, left ventricular end-diastolic dimension; LVDs, LV end-systolic dimension; IVST, interventricular septum thickness; PWT, LV diastolic posterior wall thickness; FS, fractional shortening. Values are expressed as means ± standard errors.
[b] **, $P < 0.01$ compared with sex-matched NTg mice.

sion in embryonic and neonatal hearts of Tg-MURC mice was not altered compared with that in embryonic and neonatal hearts of NTg mice, respectively. However, ANP mRNA expression increased in adult hearts of Tg-MURC mice compared with NTg mice. Furthermore, although in NTg mice ANP mRNA expression decreased in adult hearts compared with neonatal hearts, which is consistent with a previous report (24), in Tg-MURC mice ANP mRNA expression increased in adult hearts compared with neonatal hearts. Since we used the αMHC promoter to generate Tg-MURC mice, most of the exogenous MURC gene driven by the αMHC promoter in the hearts of Tg-MURC mice would be expressed after birth. Taken together, our findings suggest that sustained overexpression of MURC in the postnatal heart regulates ANP expression in vivo.

DISCUSSION

We demonstrated MURC as a novel molecule localized to the cytoplasm and partly in the Z-line of the sarcomere in the heart. MURC mRNA was expressed in heart, skeletal muscle, and vascular smooth muscle. In vascular smooth muscle cells, which have no Z-disc, MURC protein was diffusely localized to the cytoplasm, suggesting that MURC is normally localized to the cytoplasm in addition to the Z-disc. We also identified SDPR as a MURC-binding protein. Exogenous SDPR was observed in the cytoplasm of cardiomyocytes. SDPR has been shown to be phosphorylated by PKC and to be localized to the cytoplasm (18). SDPR has been identified also as a PKCα-binding protein involved in the targeting of PKCα to caveolae (30). Caveolae have been suggested to be implicated in many cellular processes, including transcytosis of macromolecules, cholesterol transport, and signal transduction (15). Signaling through the caveolae is considered to be involved in the pathogenesis of the cardiovascular system (15). In cardiomyocytes, initiation and transduction of stretch-induced RhoA activation through caveloae have been reported (27). We demonstrated in the present study that MURC induced RhoA activation in vitro and in vivo. MURC also induced ANP mRNA expression and myofibrillar organization in cardiomyocytes, both of which were mediated by Rho/ROCK pathways. Furthermore, overexpression of SDPR in cardiomyocytes augmented MURC-induced transactivation of the ANP promoter, while RNAi-mediated knockdown of SDPR attenuated it. These findings suggest that in cardiomyocytes MURC functions as a molecule that shuttles between the Z-disc and other subcellular locations to transmit signals and that MURC requires SDPR to function efficiently in cardiomyocytes.

In addition to the activation of RhoA induced by MURC in vitro and in vivo, the cardiac phenotype of Tg-MURC mice was similar to that of transgenic mice expressing RhoA (37). These findings suggest that RhoA acts as one of the important downstream effectors of MURC in the heart. The Rho GTPase cycles between GDP-bound inactive and GTP-bound active forms (12). The nucleotide state of Rho GTPases is regulated by three kinds of regulators: guanine nucleotide exchange factors, GTPase-activating proteins, and Rho GDP dissociation inhibitors. Since MURC contains no recognizable protein motifs except for the coiled-coil motif, MURC probably interacts with molecules that directly or indirectly regulate the activity of upstream regulators for RhoA. The RhoA signaling pathway is activated by G protein-coupled receptor agonists angiotensin II and PE in cardiomyocytes (3, 23). The results shown here that MURC mediates PE-induced ANP mRNA expression and myofibrillar organization suggest the involvement of a MURC-regulated Rho/ROCK pathway. Taken together, our findings indicate that MURC per se causes signaling events to induce gene expression and myofibrillar organization, and MURC also serves to transmit signals from cell surface receptors.

Responsiveness to MURC signaling in the ANP promoter required the SRE sites, suggesting that MURC signaling regulates SRF transcriptional activity. Cardiac-specific transgenic mice expressing SRF develop severe heart failure accompanied by activation of the fetal gene program, cardiac hypertrophy, chamber dilatation, and interstitial fibrosis (49). Cardiac-specific overexpression of a mutant form of SRF that reduces the binding activity to SRE sites causes dilated cardiomyopathy (50), and deletion of SRF from the adult heart also shows dilated cardiomyopathy (34). These studies indicate that the function of SRF is critical for maintaining cardiac function in

TABLE 3. Hemodynamic analysis of NTg and Tg-MURC mice[a]

Mice (n)	HR (bpm)	SBP (mm Hg)	DBP (mm Hg)	LVEDP (mm Hg)	Max dP/dt (mm Hg/s)	Min dP/dt (mm Hg/s)	τ (ms)
NTg (4)	565 ± 2	87.5 ± 4.4	60.0 ± 5.6	6.6 ± 0.7	7,913 ± 572	−7,294 ± 534	8.2 ± 1.1
Tg-MURC[b] (6)	468 ± 15**	81.8 ± 3.8	54.5 ± 2.9	9.3 ± 1.2	5,599 ± 426*	−6,011 ± 599	16.1 ± 7.4

[a] HR, heart rate; SBP, systolic blood pressure; DBP, diastolic blood pressure; LVEDP, left ventricular end-diastolic pressure; Max dP/dt, maximum LV dP/dt; Min dP/dt, minimum LV dP/dt; τ, time constant estimated from isovolumic LV pressure decay. Values are expressed as means ± standard errors.
[b] **, $P < 0.01$; *, $P < 0.05$ (compared with sex-matched NTg mice).

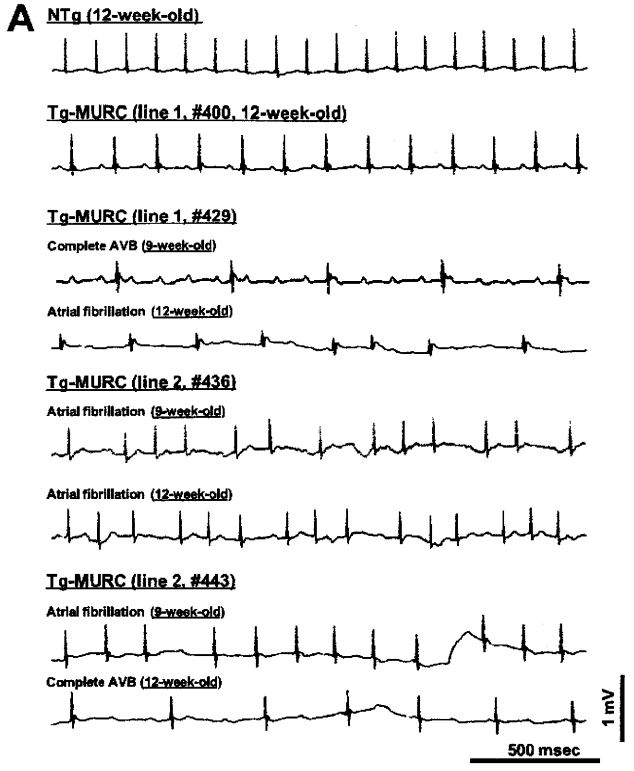

B

	NTg (n=9)	Tg-MURC (n=9)
HR (bpm)	516 ± 30	400 ± 17**
PR interval (msec)	43.89 ± 1.39	57.78 ± 1.47**

FIG. 10. Conduction disturbance and increased vulnerability to atrial arrhythmias in transgenic mice expressing MURC. (A) Representative ECG recordings from anesthetized NTg and Tg-MURC mice. ECG samples of Tg-MURC mice are shown at 9 and 12 weeks of age. (B) Tg-MURC mice have a slow heart rate and prolongation of the PR interval. ECG data were collected at 12 weeks of age. **, $P < 0.01$ compared with NTg mice. AVB, atrioventricular block; HR, heart rate.

the postnatal heart. Since Tg-MURC mice also exhibited a partly similar cardiac phenotype to transgenic mice expressing SRF, SRF transcriptional activation by MURC could contribute to the cardiac phenotype observed in Tg-MURC mice.

The striated muscle activator of Rho signaling (STARS) protein has been identified as a muscle-specific actin-binding protein localized to the I-band and the M-line of the sarcomere (4). STARS stimulates the transcriptional activity of SRF. STARS expression in the heart has been shown to be upregulated in mouse models of cardiac hypertrophy and in human cardiomyopathy, and cardiac overexpression of STARS sensitizes the heart to biomechanical stress induced by transverse aortic banding and calcineurin signaling (28). Since the localization of STARS abuts the Z-line on both sides (4), STARS appears not to be colocalized with MURC in cardiomyocytes. However, with regard to the Rho/ROCK pathway, MURC signaling overlaps with STARS signaling. Transgenic mice expressing STARS without biomechanical stress have been reported to show no cardiac dysfunction and no histological

TABLE 4. Changes in gene expression in hearts of Tg-MURC mice[a]

Symbol	Name	Fold increase
Nppa	Natriuretic peptide precursor type A (ANP)	39.00 ± 1.50**
Nppb	Natriuretic peptide precursor type B (BNP)	11.15 ± 1.21**
Myh6	Myosin, heavy polypeptide 6, cardiac muscle, alpha (αMHC)	0.91 ± 0.06
Myh7	Myosin, heavy polypeptide 7, cardiac muscle, beta (βMHC)	14.04 ± 2.13**
Atp2a2	ATPase, Ca transporting, cardiac muscle, slow twitch 2 (SERCA2)	0.74 ± 0.00**
Tgfb1	Transforming growth factor β1	1.50 ± 0.04*
Tgfb2	Transforming growth factor β2	27.36 ± 1.92**
Tgfb3	Transforming growth factor β3	3.30 ± 0.30**
Col1a1	Procollagen, type I α1	4.92 ± 0.92*
Col1a2	Procollagen, type I α2	3.80 ± 0.27**
Col3a1	Procollagen, type III α1	4.96 ± 0.89*

[a] Results shown are the ratios of gene expression in the hearts of Tg-MURC relative to NTg mice ($n = 3$). *, $P < 0.05$ compared with NTg mice; **, $P < 0.01$ compared with NTg mice.

abnormality (28). Tg-MURC mice spontaneously showed cardiac dysfunction and histological abnormality. The phenotypic difference between these mice may be caused by the action on the Rho/ROCK pathway and/or the functions that are dependent on their localization.

MURC expression in the heart increased during the developmental process from the embryonic stage to adulthood. Furthermore, in the postnatal heart MURC expression was upregulated in the hypertrophied heart. These results indicate that MURC expression is regulated under both physiological and pathological conditions. Tg-MURC mice showed cardiac contractile dysfunction and conduction disturbances with increased vulnerability to atrial arrhythmias, which was associated with an altered cardiac gene expression profile resembling that in pressure-overloaded mice but not in exercised mice (29). In Tg-MURC mice at 5 weeks of age, various sizes of cardiomyocytes were observed in Tg-MURC mice. These findings suggest that sustained overexpression of MURC in the postnatal heart causes pathological gene expression and that the expression level of MURC in the postnatal heart is critical for the maintenance of cardiac function and arrhythmogenesis. Increased inducibility of AF has been demonstrated in animal models of aging, congestive HF (CHF), atrial fibrosis, cardiac-specific overexpression of Rho A and constitutively active Rac1, and connexin 40 deficiency (1, 11, 19, 37). Atrial fibrosis

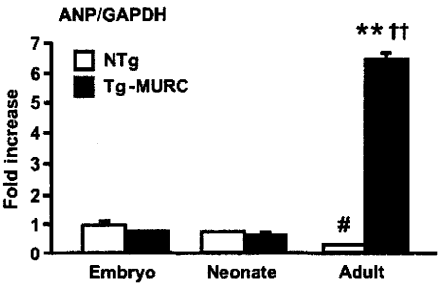

FIG. 11. ANP mRNA expression in embryonic, neonatal, and adult hearts of NTg and Tg-MURC mice. Real-time RT-PCR was performed with cDNAs from embryonic (E10.5), neonatal, and adult hearts of NTg and Tg-MURC mice. **, $P < 0.01$ compared with Tg-MURC embryo at E10.5; ††, $P < 0.01$ compared with NTg adult; #, $P < 0.05$ compared with NTg neonate.

increases with age in humans and is observed in patients with AF and in animal models of aging, CHF, and cardiac-specific overexpression of TGF-β1, tumor necrosis factor alpha, and angiotensin-converting enzyme (11, 36, 38, 46, 48). Genes involved in fibrosis, such as TGF-β and procollagens, were upregulated in the hearts of Tg-MURC mice, which also exhibited diffuse atrial fibrosis and spontaneous episodes of AF. Therefore, susceptibility to fibrosis is likely attributed to an increased vulnerability to AF in MURC-Tg mice. Our findings also suggest the critical role of MURC in the development of a vulnerable substrate for AF, especially in the setting of CHF.

In conclusion, the present study demonstrates that MURC is a Z-line-localizing molecule and it modulates the Rho/ROCK signaling pathway. Sustained overexpression of MURC facilitates functional deterioration, including cardiac function and conduction disturbances. Further investigation of the role of MURC will provide insights into the molecular mechanisms of the Z-disc that regulate cardiac homeostasis and pathogenesis.

ACKNOWLEDGMENTS

We thank M. Kuramoto, M. Nishikawa, A. Kosugi, and A. Yasui for their technical assistance. We also thank the following investigators for their kind gifts of plasmids: Jeffrey Robbins, Kenneth R. Chien, Andrew Thorburn, Yoshimi Takai, and Seigo Izumo.

This work was supported by grants-in-aid from the Ministry of Education, Culture, Sports, Science, and Technology of Japan, Japan Association for the Advancement of Medical Equipment, Takeda Science Foundation, and Mitsubishi Pharma Research Foundation.

REFERENCES

1. **Adam, O., G. Frost, F. Custodis, M. A. Sussman, H. J. Schafers, M. Bohm, and U. Laufs.** 2007. Role of Rac1 GTPase activation in atrial fibrillation. J. Am. Coll. Cardiol. **50:**359–367.
2. **Amano, M., Y. Fukata, and K. Kaibuchi.** 2000. Regulation and functions of Rho-associated kinase. Exp. Cell. Res. **261:**44–51.
3. **Aoki, H., S. Izumo, and J. Sadoshima.** 1998. Angiotensin II activates RhoA in cardiac myocytes: a critical role of RhoA in angiotensin II-induced premyofibril formation. Circ. Res. **82:**666–676.
4. **Arai, A., J. A. Spencer, and E. N. Olson.** 2002. STARS, a striated muscle activator of Rho signaling and serum response factor-dependent transcription. J. Biol. Chem. **277:**24453–24459.
5. **Burgener, R., M. Wolf, T. Ganz, and M. Baggiolini.** 1990. Purification and characterization of a major phosphatidylserine-binding phosphoprotein from human platelets. Biochem. J. **269:**729–734.
6. **Chihara, K., M. Amano, N. Nakamura, T. Yano, M. Shibata, T. Tokui, H. Ichikawa, R. Ikebe, M. Ikebe, and K. Kaibuchi.** 1997. Cytoskeletal rearrangements and transcriptional activation of c-fos serum response element by Rho-kinase. J. Biol. Chem. **272:**25121–25127.
7. **Churchill, E., G. Budas, A. Vallentin, T. Koyanagi, and D. Mochly-Rosen.** 2008. PKC isozymes in chronic cardiac disease: possible therapeutic targets? Annu. Rev. Pharmacol. Toxicol. **48:**569–599.
8. **Clark, K. A., A. S. McElhinny, M. C. Beckerle, and C. C. Gregorio.** 2002. Striated muscle cytoarchitecture: an intricate web of form and function. Annu. Rev. Cell Dev. Biol. **18:**637–706.
9. **Epstein, N. D., and J. S. Davis.** 2003. Sensing stretch is fundamental. Cell **112:**147–150.
10. **Etienne-Manneville, S., and A. Hall.** 2002. Rho GTPases in cell biology. Nature **420:**629–635.
11. **Everett, T. H. T., and J. E. Olgin.** 2007. Atrial fibrosis and the mechanisms of atrial fibrillation. Heart Rhythm **4:**S24–S27.
12. **Fukata, M., M. Nakagawa, and K. Kaibuchi.** 2003. Roles of Rho-family GTPases in cell polarisation and directional migration. Curr. Opin. Cell Biol. **15:**590–597.
13. **Fuster, V., L. E. Ryden, D. S. Cannom, H. J. Crijns, A. B. Curtis, K. A. Ellenbogen, J. L. Halperin, J. Y. Le Heuzey, G. N. Kay, J. E. Lowe, S. B. Olsson, E. N. Prystowsky, J. L. Tamargo, S. Wann, S. C. Smith, Jr., A. K. Jacobs, C. D. Adams, J. L. Anderson, E. M. Antman, S. A. Hunt, R. Nishimura, J. P. Ornato, R. L. Page, B. Riegel, S. G. Priori, J. J. Blanc, A. Budaj, A. J. Camm, V. Dean, J. W. Deckers, C. Despres, K. Dickstein, J. Lekakis, K. McGregor, M. Metra, J. Morais, A. Osterspey, and J. L. Zamorano.** 2006. ACC/AHA/ESC 2006 guidelines for the management of patients with atrial fibrillation, executive summary: a report of the American College of Cardiology/American Heart Association Task Force on Practice Guidelines and the European Society of Cardiology Committee for Practice Guidelines (Writing Committee to Revise the 2001 Guidelines for the Management of Patients with Atrial Fibrillation). J. Am. Coll. Cardiol. **48:**854–906.
14. **Geneste, O., J. W. Copeland, and R. Treisman.** 2002. LIM kinase and Diaphanous cooperate to regulate serum response factor and actin dynamics. J. Cell Biol. **157:**831–838.
15. **Gratton, J. P., P. Bernatchez, and W. C. Sessa.** 2004. Caveolae and caveolins in the cardiovascular system. Circ. Res. **94:**1408–1417.
16. **Gulick, J., A. Subramaniam, J. Neumann, and J. Robbins.** 1991. Isolation and characterization of the mouse cardiac myosin heavy chain genes. J. Biol. Chem. **266:**9180–9185.
17. **Gustincich, S., and C. Schneider.** 1993. Serum deprivation response gene is induced by serum starvation but not by contact inhibition. Cell Growth Differ. **4:**753–760.
18. **Gustincich, S., P. Vatta, S. Goruppi, M. Wolf, S. Saccone, G. Della Valle, M. Baggiolini, and C. Schneider.** 1999. The human serum deprivation response gene (SDPR) maps to 2q32-q33 and codes for a phosphatidylserine-binding protein. Genomics **57:**120–129.
19. **Hagendorff, A., B. Schumacher, S. Kirchhoff, B. Luderitz, and K. Willecke.** 1999. Conduction disturbances and increased atrial vulnerability in Connexin40-deficient mice analyzed by transesophageal stimulation. Circulation **99:**1508–1515.
20. **Hill, C. S., J. Wynne, and R. Treisman.** 1995. The Rho family GTPases RhoA, Rac1, and CDC42Hs regulate transcriptional activation by SRF. Cell **81:**1159–1170.
21. **Hines, W. A., J. Thorburn, and A. Thorburn.** 1999. A low-affinity serum response element allows other transcription factors to activate inducible gene expression in cardiac myocytes. Mol. Cell. Biol. **19:**1841–1852.
22. **Hoshijima, M.** 2006. Mechanical stress-strain sensors embedded in cardiac cytoskeleton: Z disk, titin, and associated structures. Am. J. Physiol. Heart Circ. Physiol. **290:**H1313–H1325.
23. **Hoshijima, M., V. P. Sah, Y. Wang, K. R. Chien, and J. H. Brown.** 1998. The low molecular weight GTPase Rho regulates myofibril formation and organization in neonatal rat ventricular myocytes. Involvement of Rho kinase. J. Biol. Chem. **273:**7725–7730.
24. **Houweling, A. C., M. M. van Borren, A. F. Moorman, and V. M. Christoffels.** 2005. Expression and regulation of the atrial natriuretic factor encoding gene Nppa during development and disease. Cardiovasc. Res. **67:**583–593.
25. **Kasahara, H., T. Ueyama, H. Wakimoto, M. K. Liu, C. T. Maguire, K. L. Converso, P. M. Kang, W. J. Manning, J. Lawitts, D. L. Paul, C. I. Berul, and S. Izumo.** 2003. Nkx2.5 homeoprotein regulates expression of gap junction protein connexin 43 and sarcomere organization in postnatal cardiomyocytes. J. Mol. Cell. Cardiol. **35:**243–256.
26. **Kasahara, H., H. Wakimoto, M. Liu, C. T. Maguire, K. L. Converso, T. Shioi, W. Y. Huang, W. J. Manning, D. Paul, J. Lawitts, C. I. Berul, and S. Izumo.** 2001. Progressive atrioventricular conduction defects and heart failure in mice expressing a mutant Csx/Nkx2.5 homeoprotein. J. Clin. Investig. **108:**189–201.
27. **Kawamura, S., S. Miyamoto, and J. H. Brown.** 2003. Initiation and transduction of stretch-induced RhoA and Rac1 activation through caveolae: cytoskeletal regulation of ERK translocation. J. Biol. Chem. **278:**31111–31117.
28. **Kuwahara, K., G. C. Teg Pipes, J. McAnally, J. A. Richardson, J. A. Hill, R. Bassel-Duby, and E. N. Olson.** 2007. Modulation of adverse cardiac remodeling by STARS, a mediator of MEF2 signaling and SRF activity. J. Clin. Investig. **117:**1324–1334.
29. **McMullen, J. R., T. Shioi, L. Zhang, O. Tarnavski, M. C. Sherwood, P. M. Kang, and S. Izumo.** 2003. Phosphoinositide 3-kinase(p110α) plays a critical role for the induction of physiological, but not pathological, cardiac hypertrophy. Proc. Natl. Acad. Sci. USA **100:**12355–12360.
30. **Mineo, C., Y. S. Ying, C. Chapline, S. Jaken, and R. G. Anderson.** 1998. Targeting of protein kinase Cα to caveolae. J. Cell Biol. **141:**601–610.
31. **Muslin, A. J.** 2005. Role of Raf proteins in cardiac hypertrophy and cardiomyocyte survival. Trends Cardiovasc. Med. **15:**225–229.
32. **Narumiya, S., and S. Yasuda.** 2006. Rho GTPases in animal cell mitosis. Curr. Opin. Cell Biol. **18:**199–205.
33. **Ogata, T., T. Ueyama, T. Nomura, S. Asada, M. Tagawa, T. Nakamura, T. Takahashi, H. Matsubara, and H. Oh.** 2007. Osteopontin is a myosphere-derived secretory molecule that promotes angiogenic progenitor cell proliferation through the phosphoinositide 3-kinase/Akt pathway. Biochem. Biophys. Res. Commun. **359:**341–347.
34. **Parlakian, A., C. Charvet, B. Escoubet, M. Mericskay, J. D. Molkentin, G. Gary-Bobo, L. J. De Windt, M. A. Ludosky, D. Paulin, D. Daegelen, D. Tuil, and Z. Li.** 2005. Temporally controlled onset of dilated cardiomyopathy through disruption of the SRF gene in adult heart. Circulation **112:**2930–2939.
35. **Pyle, W. G., and R. J. Solaro.** 2004. At the crossroads of myocardial signaling: the role of Z-discs in intracellular signaling and cardiac function. Circ. Res. **94:**296–305.
36. **Saba, S., A. M. Janczewski, L. C. Baker, V. Shusterman, E. C. Gursoy, A. M. Feldman, G. Salama, C. F. McTiernan, and B. London.** 2005. Atrial contractile dysfunction, fibrosis, and arrhythmias in a mouse model of cardio-

myopathy secondary to cardiac-specific overexpression of tumor necrosis factor-α. Am. J. Physiol. Heart Circ. Physiol. **289:**H1456–H1467.
37. **Sah, V. P., S. Minamisawa, S. P. Tam, T. H. Wu, G. W. Dorn, 2nd, J. Ross, Jr., K. R. Chien, and J. H. Brown.** 1999. Cardiac-specific overexpression of RhoA results in sinus and atrioventricular nodal dysfunction and contractile failure. J. Clin. Investig. **103:**1627–1634.
38. **Sawaya, S. E., Y. S. Rajawat, T. G. Rami, G. Szalai, R. L. Price, N. Sivasubramanian, D. L. Mann, and D. S. Khoury.** 2007. Downregulation of connexin 40 and increased prevalence of atrial arrhythmias in transgenic mice with cardiac-restricted overexpression of tumor necrosis factor. Am. J. Physiol. Heart Circ. Physiol. **292:**H1561–H1567.
39. **Shioi, T., P. M. Kang, P. S. Douglas, J. Hampe, C. M. Yballe, J. Lawitts, L. C. Cantley, and S. Izumo.** 2000. The conserved phosphoinositide 3-kinase pathway determines heart size in mice. EMBO J. **19:**2537–2548.
40. **Stace, C. L., and N. T. Ktistakis.** 2006. Phosphatidic acid- and phosphatidylserine-binding proteins. Biochim. Biophys. Acta **1761:**913–926.
41. **Ueyama, T., H. Kasahara, T. Ishiwata, Q. Nie, and S. Izumo.** 2003. Myocardin expression is regulated by Nkx2.5, and its function is required for cardiomyogenesis. Mol. Cell. Biol. **23:**9222–9232.
42. **Ueyama, T., H. Kasahara, T. Ishiwata, N. Yamasaki, and S. Izumo.** 2003. Csm, a cardiac-specific isoform of the RNA helicase Mov10l1, is regulated by Nkx2.5 in embryonic heart. J. Biol. Chem. **278:**28750–28757.
43. **Ueyama, T., S. Kawashima, T. Sakoda, Y. Rikitake, T. Ishida, M. Kawai, T. Yamashita, S. Ishido, H. Hotta, and M. Yokoyama.** 2000. Requirement of activation of the extracellular signal-regulated kinase cascade in myocardial cell hypertrophy. J. Mol. Cell. Cardiol. **32:**947–960.
44. **Ueyama, T., T. Sakoda, S. Kawashima, E. Hiraoka, K. Hirata, H. Akita, and M. Yokoyama.** 1997. Activated RhoA stimulates c-fos gene expression in myocardial cells. Circ. Res. **81:**672–678.
45. **Velculescu, V. E., B. Vogelstein, and K. W. Kinzler.** 2000. Analysing uncharted transcriptomes with SAGE. Trends Genet. **16:**423–425.
46. **Verheule, S., T. Sato, T. t. Everett, S. K. Engle, D. Otten, M. Rubart-von der Lohe, H. O. Nakajima, H. Nakajima, L. J. Field, and J. E. Olgin.** 2004. Increased vulnerability to atrial fibrillation in transgenic mice with selective atrial fibrosis caused by overexpression of TGF-β1. Circ. Res. **94:**1458–1465.
47. **Wei, L., G. E. Taffet, D. S. Khoury, J. Bo, Y. Li, A. Yatani, M. C. Delaughter, R. Klevitsky, T. E. Hewett, J. Robbins, L. H. Michael, M. D. Schneider, M. L. Entman, and R. J. Schwartz.** 2004. Disruption of Rho signaling results in progressive atrioventricular conduction defects while ventricular function remains preserved. FASEB J. **18:**857–859.
48. **Xiao, H. D., S. Fuchs, D. J. Campbell, W. Lewis, S. C. Dudley, Jr., V. S. Kasi, B. D. Hoit, G. Keshelava, H. Zhao, M. R. Capecchi, and K. E. Bernstein.** 2004. Mice with cardiac-restricted angiotensin-converting enzyme (ACE) have atrial enlargement, cardiac arrhythmia, and sudden death. Am. J. Pathol. **165:**1019–1032.
49. **Zhang, X., G. Azhar, J. Chai, P. Sheridan, K. Nagano, T. Brown, J. Yang, K. Khrapko, A. M. Borras, J. Lawitts, R. P. Misra, and J. Y. Wei.** 2001. Cardiomyopathy in transgenic mice with cardiac-specific overexpression of serum response factor. Am. J. Physiol. Heart Circ. Physiol. **280:**H1782–H1792.
50. **Zhang, X., J. Chai, G. Azhar, P. Sheridan, A. M. Borras, M. C. Furr, K. Khrapko, J. Lawitts, R. P. Misra, and J. Y. Wei.** 2001. Early postnatal cardiac changes and premature death in transgenic mice overexpressing a mutant form of serum response factor. J. Biol. Chem. **276:**40033–40040.

Circulation
JOURNAL OF THE AMERICAN HEART ASSOCIATION

Central Role of Calcium-Dependent Tyrosine Kinase PYK2 in Endothelial Nitric Oxide Synthase Mediated Angiogenic Response and Vascular Function

Akihiro Matsui, Mitsuhiko Okigaki, Katsuya Amano, Yasushi Adachi, Denan Jin, Shinji Takai, Tomoya Yamashita, Seinosuke Kawashima, Tatsuya Kurihara, Mizuo Miyazaki, Kento Tateishi, Shinsaku Matsunaga, Asako Katsume, Shoken Honshou, Tomosaburo Takahashi, Satoaki Matoba, Tetsuro Kusaba, Tetsuya Tatsumi and Hiroaki Matsubara

Circulation 2007;116;1041-1051; originally published online Aug 13, 2007;
DOI: 10.1161/CIRCULATIONAHA.106.645416
Circulation is published by the American Heart Association. 7272 Greenville Avenue, Dallas, TX 72514
 Print ISSN: 0009-7322. Online ISSN: 1524-4539

Central Role of Calcium-Dependent Tyrosine Kinase PYK2 in Endothelial Nitric Oxide Synthase–Mediated Angiogenic Response and Vascular Function

Akihiro Matsui, MD; Mitsuhiko Okigaki, MD, PhD; Katsuya Amano, MD, PhD; Yasushi Adachi, MD, PhD; Denan Jin, MD, PhD; Shinji Takai, PhD; Tomoya Yamashita, MD, PhD; Seinosuke Kawashima, MD, PhD; Tatsuya Kurihara, PhD; Mizuo Miyazaki, MD, PhD; Kento Tateishi, MD, PhD; Shinsaku Matsunaga, MD; Asako Katsume, MD; Shoken Honshou, MD; Tomosaburo Takahashi, MD, PhD; Satoaki Matoba, MD, PhD; Tetsuro Kusaba, MD; Tetsuya Tatsumi, MD, PhD; Hiroaki Matsubara, MD, PhD

Background—The involvement of Ca^{2+}-dependent tyrosine kinase PYK2 in the Akt/endothelial NO synthase pathway remains to be determined.

Methods and Results—Blood flow recovery and neovessel formation after hind-limb ischemia were impaired in $PYK2^{-/-}$ mice with reduced mobilization of endothelial progenitors. Vascular endothelial growth factor (VEGF)–mediated cytoplasmic Ca^{2+} mobilization and Ca^{2+}-independent Akt activation were markedly decreased in the PYK2-deficient aortic endothelial cells, whereas the Ca^{2+}-independent AMP-activated protein kinase/protein kinase-A pathway that phosphorylates endothelial NO synthase was not impaired. Acetylcholine-mediated aortic vasorelaxation and cGMP production were significantly decreased. Vascular endothelial growth factor–dependent migration, tube formation, and actin cytoskeletal reorganization associated with Rac1 activation were inhibited in PYK2-deficient endothelial cells. PI3-kinase is associated with vascular endothelial growth factor–induced PYK2/Src complex, and inhibition of Src blocked Akt activation. The vascular endothelial growth factor–mediated Src association with PLCγ1 and phosphorylation of ^{783}Tyr-PLCγ1 also were abolished by PYK2 deficiency.

Conclusion—These findings demonstrate that PYK2 is closely involved in receptor- or ischemia-activated signaling events via Src/PLCγ1 and Src/PI3-kinase/Akt pathways, leading to endothelial NO synthase phosphorylation, and thus modulates endothelial NO synthase–mediated vasoactive function and angiogenic response. (***Circulation.*** **2007;116: 1041-1051.)**

Key Words: angiogenesis ■ endothelium ■ nitric oxide synthase ■ signal transduction ■ vasodilation

Nitric oxide (NO) has multiple functions in NO-mediated vascular action and angiogenic response. This was confirmed by endothelial NO synthase $(eNOS)^{-/-}$ mice exhibiting hypertension[1] or impaired vascular endothelial growth factor (VEGF) –induced angiogenesis.[2] VEGF phosphorylates eNOS, which is directly activated on the phosphorylation of ^{1177}serine in human (^{1176}serine in mouse) by Akt,[3,4] whereas the upstream molecules that activate Akt-eNOS system have not been fully clarified.

Clinical Perspective p 1051

Tyrosine kinases activate the PI3-kinase/Akt or Ca^{2+} signaling pathways, suggesting that tyrosine kinase is upstream of eNOS. Indeed, Src and VEGF receptor-2 activate eNOS through activation of the PI3-kinase/Akt pathway.[5] PYK2 (proline-rich tyrosine kinase), also known as RAFTK, CAK, and CADTK,[6,7] is the cytoplasmic tyrosine kinase and exhibits 45% amino acid sequence

Received August 9, 2005; accepted June 12, 2007.

From the Department of Cardiovascular Medicine, Kyoto Prefectural University School of Medicine, Kyoto (A.M., M.O., K.T., S.M., A.K., S.H., T. Takahashi, S.M., T. Kusaba, T. Tatsumi, H.M.); Departments of Internal Medicine II (K.A.) and Pathology I (Y.A.), Kansai Medical University, Osaka; Department of Pharmacology, Osaka Medical College, Takatsuki (D.J., S.T., M.M.); Division of Cardiovascular and Respiratory Medicine, Kobe University School of Medicine, Kobe (T.Y., S.K.); and Daiichi Asubio Pharma Co Ltd Biomedical Research Laboratories, Osaka (T. Kurihara), Japan.

The online Data Supplement, consisting of an expanded Methods section and a figure, can be found with this article at http://circ.ahajournals.org/cgi/content/full/CIRCULATIONAHA.106.645416/DC1.

Correspondence to Mitsuhiko Okigaki, MD, Department of Cardiovascular Medicine, Kyoto Prefectural University of Medicine, Kamigyo-ku, Kyoto, 602–8566, Japan. E-mail okigakim@koto.kpu-m.ac.jp

Circulation **is available at http://circ.ahajournals.org** **DOI: 10.1161/CIRCULATIONAHA.106.645416**

identity to focal adhesion kinase. Tyrosine phosphorylation of PYK2 and focal adhesion kinase was triggered by integrin-mediated adhesion.[8] PYK2 was stimulated by a broad range of physiological stimuli such as stimuli for G-protein–coupled receptors that elevate intracellular Ca^{2+},[6,7] phorbol ester, inflammatory cytokines, and stress signals, including ischemia.[9] PYK2 acts in concert with Src, which links Gi- or Gq-coupled receptors, leading to the MAP kinase pathway.[10] Furthermore, PYK2 binds to proteins that interact with the cytoskeleton, suggesting a role in the regulation of cellular morphology. The phenotype of PYK2-deficient mice was recently described as having macrophages that exhibit impaired migration as a result of cytoskeleton abnormality induced by diminished Ca^{2+} mobilization and reduced activation of PI3-kinase.[11] In this study, we newly generated $PYK2^{-/-}$ mice and investigated the molecular mechanism for the effects of PYK2 on NO-mediated vascular function and angiogenic response.

Methods

Statistical Analysis

Results are expressed as mean±SEM. All data were transformed by the natural logarithm before ANOVA corresponding to each experiment. Repeated-measures ANOVA was used to analyze the time course experiment. The Scheffé test was used as the multiple comparison test. For comparisons between 2 groups, a 2-sample *t* test was performed. A value of $P< 0.05$ (2 tailed) was considered statistically significant.

Materials, construction of targeting vector, generation of $PYK2^{-/-}$ mice (Figure I of the online Data Supplement), Western blotting, immunohistochemistry, transfection of DNA plasmid, measurement of GTP-Rho and GTP-Rac, migration, tubular formation, in vivo angiogenesis, preparation of endothelial progenitor cell (EPC) –like cells, hind-limb ischemia, laser Doppler perfusion image, cGMP assay, measurement of NO metabolites and NO levels, acetylcholine (Ach)- and nitroprusside-mediated vasodilatation, measurement of cytoplasmic Ca^{2+} concentration, fluorescence-activated cell sorting, and isolation of endothelial cells (ECs) from aorta and primary culture are described in the Methods section of the online Data Supplement. C57B1/6 strain mice (SHIMIZU Laboratory Supplies, Kyoto, Japan) were used. The animal experiments were approved by our institutional review board.

The authors had full access to and take full responsibility for the integrity of the data. All authors have read and agree to the manuscript as written.

Results

Impaired eNOS/Akt Activation and Ca^{2+} Mobilization by PYK2 Deficiency

eNOS was reported to be activated by VEGF, Ach, or ischemic stress.[12] Incubation of the aorta with VEGF (100 ng/mL) phosphorylates PYK2 time dependently with a peak level around 5 minutes (Figure 1A). Ach (1 μmol/L) also caused PYK2 phosphorylation with a similar peak level, the extent of which was comparable to that in VEGF stimulation (Figure 1A). Ischemic stress time dependently increased the phosphorylation of PYK2 in the hind-limb muscle (Figure 1B). Such PYK2 phosphorylation was observed in the primary cultured aortic von Willebrand factor–positive ECs after stimulation with VEGF (100 ng/mL) and Ach (1 μmol/L) and exposure to 1% hypoxia (Figure 1C). To clarify the cell types expressing PYK2, an immunohistochemical analysis was performed. Figure 1D showed that PYK2 was present mainly in the endothelial ($CD31^+$ ECs) and medial layers (vascular smooth muscle cells) in the aorta and in the $CD31^-$ vessels in the skeletal muscle, in which a few cells in the interstitial region ($CD31^-$) also expressed PYK2.

We next examined whether the stimuli that induce PYK2 activation led to the phosphorylation of eNOS. Hind-limb ischemia causes eNOS phosphorylation in the skeletal muscle in wild-type (+/+) mice, whereas eNOS activation in the $PYK2^{-/-}$ mice was markedly inhibited (Figure 2A). Exposure of the aorta to VEGF or Ach also induced eNOS phosphorylation, whereas their activated levels were significantly diminished in the $PYK2^{-/-}$ mice (Figure 2B). Induction of eNOS phosphorylation by VEGF or Ach or exposure to 1% hypoxia also was observed (2.3- to 2.5-fold, respectively; $P<0.005$) in the wild-type aortic ECs but strongly inhibited in the PYK2-deficient ECs (Figure 2C).

The ischemia-induced Akt phosphorylation in the skeletal muscle was significantly lower in the $PYK2^{-/-}$ mice (46±3% at 2 hours, 34±3% decrease 1 day after ischemia; $P<0.01$) than the wild-type mice (Figure 2A), whereas the tyrosine phosphorylation level in VEGF receptor-2 (Flk-1) did not significantly differ between the wild-type and PYK2-deficient muscle (n=6 each; data not shown).

Akt phosphorylation in the aorta (Figure 2B) and ECs (Figure 2C) from the wild-type mice was significantly increased by VEGF stimulation (1.7±0.3-fold, $P<0.05$; and 3.0±0.7-fold, $P<0.005$, respectively), whereas Akt activation in the PYK2-deficient aorta and ECs was markedly attenuated (43±3% and 42±6% inhibition, respectively; $P<0.05$). Significant inhibition of Akt phosphorylation in ECs by PYK2 deficiency also was observed after exposure to 1% hypoxia (72±5% inhibition; $P<0.01$; Figure 2C).

We examined the involvement of AMP-activated protein kinase (AMPK)[13] and cAMP-dependent protein kinase-A (PKA),[14] known as the Ca^{2+}-independent kinase for phosphorylation of ^{1176}Ser-eNOS. The phosphorylation levels of AMPK and PKA after hind-limb ischemia did not differ significantly between $PYK2^{-/-}$ and wild-type mice (Figure 2A). Furthermore, the phosphorylation of AMPK and PKA in PYK2-deficient ECs exposed to 1% hypoxia for 18 hours also was similar to the wild-type ECs (data not shown). Akt, AMPK, and PKA showed peak phosphorylation on day 1 and at 2 hours, respectively; PKA and AMPK then reversed to baseline levels on day 7, whereas moderate activation of Akt was observed on day 7 (220±30% increase compared with basal level; Figure 2A). Neither AMPK nor PKA was activated 5 minutes after VEGF (100 ng/mL) treatment in both the wild-type and PYK2-deficient cells (data not shown), whereas dibutylic cAMP (1 mmol/L) and 5-aminoimidazole-4-carboxamide-1-β-D-riboside AICAR (1 mmol/L) apparently phosphorylated PKA and AMPK in the wild-type ECs (positive controls; data not shown). These findings suggest that Akt, rather than Ca^{2+}-independent AMPK or PKA, is involved in VEGF-mediated eNOS phosphorylation.

To prove that the reduced phosphorylation of eNOS is due directly to the loss of PYK2, we transfected GFP-tagged PYK2 plasmid to the PYK2-deficient ECs and studied by

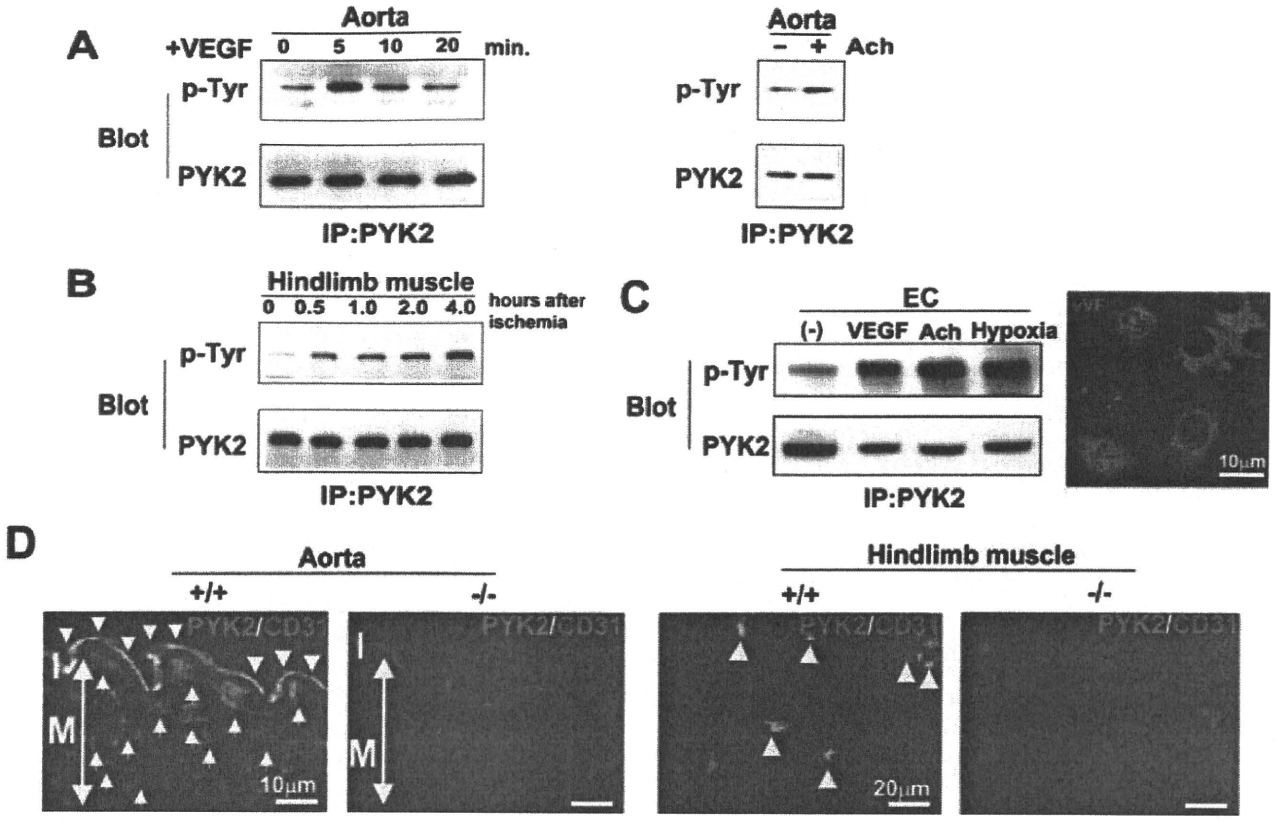

Figure 1. Activation of PYK2 by VEGF, Ach, and hind-limb ischemia. A, Aortic tissue removed from wild-type mice was incubated with the medium including VEGF (100 ng/mL) or Ach (1 μmol/L) for 5 minutes. B, Time-dependent PYK2 phosphorylation in hind-limb muscles was examined after ligation of femoral artery. C, Left, Aortic ECs were stimulated with VEGF (100 ng/mL) or Ach (1 μmol/L) for 5 minutes or exposure with 1% hypoxia for 18 hours. Tissue or cell lysates were subjected to immunoprecipitation with an anti-PYK2 antibody, followed by immunoblotting with anti-phosphotyrosine or anti-PYK2 antibodies. Data are mean±SE (n=5 each); representative results are shown. Right, Cells were immunostained with anti–von Willebrand factor antibody to identify the ECs. D, Distribution of PYK2 in the aorta and limb muscle. Aorta and limb muscle were frozen-sectioned, fixed with acetone, and subjected to double immunostaining with antibodies against PYK2 (green) and CD31 (red). The merged cells (yellow) are indicated by arrowheads; PYK2-positive smooth muscle in the aorta, by arrows. I indicates intima; M, media.

immunostaining with anti–phospho-^{1176}Ser-eNOS antibody whether VEGF-mediated phosphorylation of eNOS can be restored (Figure 2D). eNOS phosphorylation was observed in VEGF-exposed cells in which GFP-tagged PYK2 plasmid was transfected, whereas phospho-eNOS–positive cells were barely detected in the control GFP-transfected cells.

We next studied whether intracellular Ca^{2+} mobilization was influenced by PYK2 deficiency. Figure 3A shows that VEGF-mediated elevation of cytoplasmic Ca^{2+} levels was markedly inhibited in the PYK2-deficient ECs (Ca^{2+} concentrations in PYK2$^{-/-}$, 95±24 nmol/L versus wild type, 432±69 nmol/L; $P<0.001$), whereas Ca^{2+} mobilization with ATP that directly opens the Ca^{2+} channel on the plasma membrane[15] was comparable to the wild type (Figure 3A), suggesting that the pathway for the receptor-independent Ca^{2+} mobilization is not impaired. To study the effect of PYK2 deficiency on the other Ca^{2+} signaling pathway not involving NO formation, we studied the activation of the Ca^{2+}-dependent transcription factor nuclear factor of activated T cells 2 (NFATc2), which was shown to be crucial for VEGF-mediated angiogenesis.[16] The results showed that 68±8% of the wild-type cells showed nuclear translocation of NFATc2 from cytoplasm 30 minutes after VEGF stimulation, whereas in the PYK2-deficient cells, the translocation was markedly reduced (22±6%; $P<0.01$), indicating that PYK2 deficiency inhibits Ca^{2+} signaling pathway not involving NO formation (Figure 3B). To prove that the functional effects are due directly to the loss of PYK2, we transfected the GFP-tagged PYK2 plasmid to the PYK2-deficient cells and observed VEGF-mediated nuclear translocation of NFATc2. In the PYK2-deficient cells transfected with GFP-tagged PYK2 plasmid, the number of NFATc2-translocated cells increased significantly (from 22±6% to 48±9%; $P<0.05$; Figure 3B), whereas in the control GFP-transfected cells, the translocated cells did not increase significantly (data not shown). Pretreatment with a chelator of intracellular Ca^{2+} store, AM-BAPTA (5 μmol/L), in the Ca^{2+}-free medium for 45 minutes did not affect VEGF-induced Akt activation in ECs (Figure 3C), indicating that Akt activation is Ca^{2+} independent in our system.

Reduced Response by PYK2 Deficiency in NO Production and Ach-Mediated Vasodilatation

The intracellular NO level was measured with 4-amino-5-methyl-amino-2′,7′-difluorofluorescein diacetate (DAF-FM DA). NO was visualized as green under laser

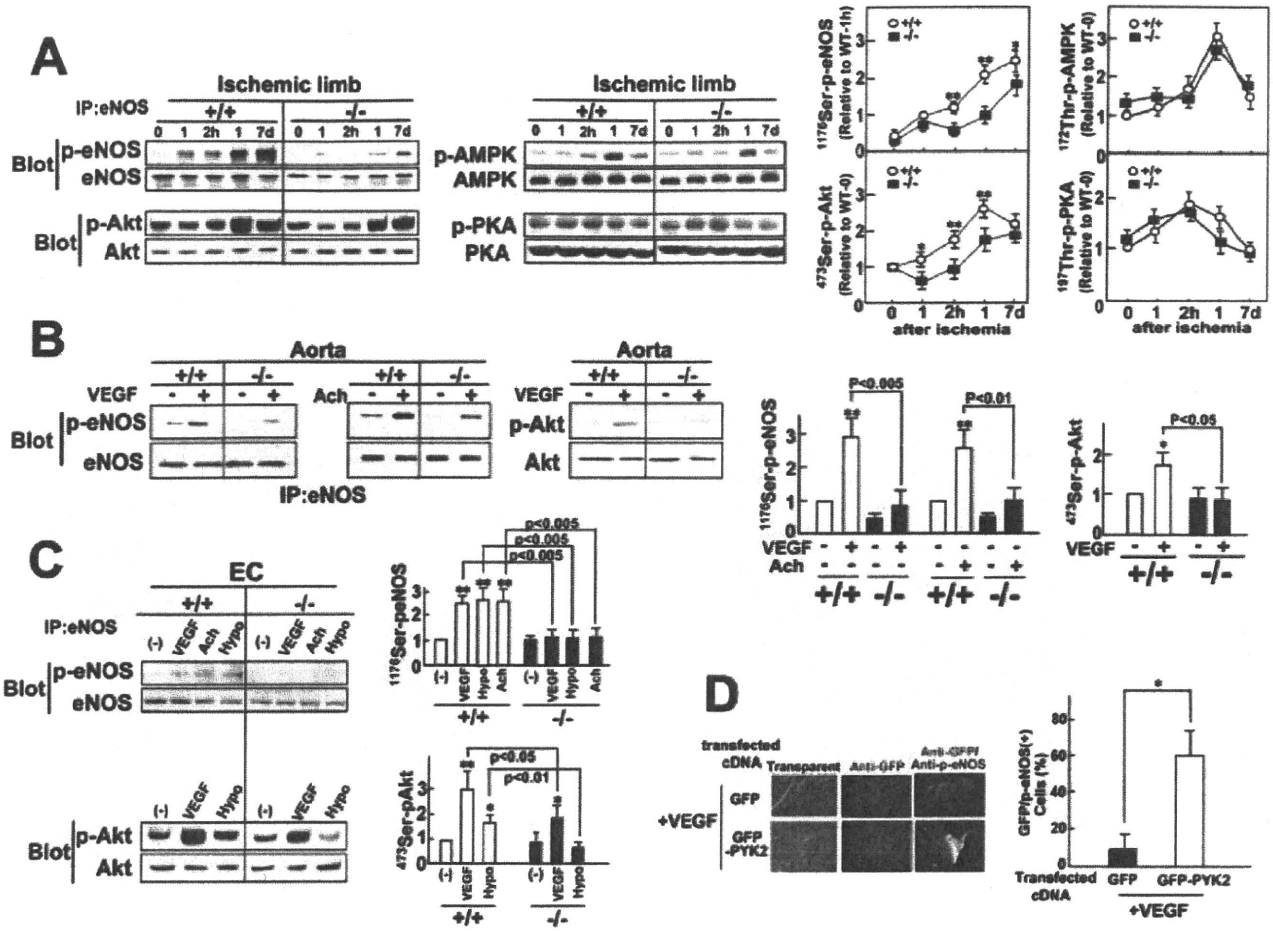

Figure 2. Impaired eNOS/Akt activation in PYK2-deficient mice. A, Skeletal muscle (n=10) was excised at the indicated time after ischemia. B, Aortic tissue (n=6 for each stimuli) was stimulated with VEGF (100 ng/mL) or Ach (1 μmol/L) for 5 minutes. C, Aortic ECs (n=6 for each stimuli) were stimulated with VEGF (100 ng/mL) or Ach (1 μmol/L) for 5 minutes or 1% hypoxia for 18 hours (n=6 each). Cell lysates were subjected to immunoprecipitation with anti-eNOS antibody, followed by immunoblot with antibodies against ^{1176}Ser-phosphorylated eNOS or eNOS. In addition, lysates were immunoblotted with antibodies against ^{473}Ser-phosphorylated Akt or Akt. Relative phosphorylation levels of eNOS and Akt are shown. Open circles and closed squares indicate the wild-type and PYK2$^{-/-}$ mice, respectively. A, $^{*}P<0.05$, $^{**}P<0.01$ vs the same time points of the PYK2$^{-/-}$ mice. B, C, $^{*}P<0.05$, $^{**}P<0.005$ vs the nonstimulated control. D, Aortic ECs were transfected with GFP- or GFP-PYK2-cDNA-plasmid. Forty-eight hours after transfection, cells were stimulated with VEGF (100 ng/mL), fixed with 4% paraformaldehyde, permeabilized with 0.02% Triton/PBS, and immunostained with antibodies against GFP- (red) or ^{1176}Ser-phosphorylated eNOS (green). Ratio of the GFP/p-eNOS double-positive cells (%) (yellow) to the total GFP-positive cells (red) was evaluated. $^{*}P<0.005$; n=4.

microscopy (Figure 4A). In the wild-type ECs, VEGF increased NO levels by 3.2-fold ($P<0.005$ versus untreated cells), whereas this increase was severely impaired in the PYK2-deficient ECs. NO metabolites in the 24-hour urine sample were significantly lower in the PYK2$^{-/-}$ mice than the wild-type mice (4084±820 versus 9326±1163 nmol; $P<0.005$; Figure 4B). Oral administration of N^{G}-nitro-L-arginine methyl ester (L-NAME; 3 mmol/L in drinking water) to the wild-type mice reduced the NO metabolite production to a level comparable to the PYK2$^{-/-}$ mice (Figure 4B).

Ach-mediated vasodilatation is induced by the eNOS-NO system. We next examined whether Ach-mediated relaxation of the aorta is influenced by PYK2 deficiency. The dose-dependent relaxation of the isolated aorta constricted by norepinephrine was evaluated (Figure 4C). Ach (10 μmol/L) -mediated relaxation response was much weaker in the PYK2-deficient aorta than in the wild-type aorta (32±8% versus 59±5% relaxation; $P<0.01$), whereas norepinephrine (300 nmol/L) -mediated vasoconstriction in the PYK2-deficient aorta did not significantly differ from the wild-type aorta (190±30% versus 165±6% relative to 50 mmol/L KCl–mediated constriction; n=5). This result suggests that Ca^{2+} signaling transmitted mainly through voltage-dependent Ca^{2+} channel leading to the constriction of vascular smooth muscle cells is not impaired in the PYK2-deficient aorta.

To evaluate the NO dependency on Ach-mediated vasorelaxation, the effect of L-NAME was studied. Addition of L-NAME (10 μmol/L) markedly suppressed the Ach-mediated maximum relaxation of the wild-type aorta (from 59±5% to 17±2%; $P<0.001$; n=4), whereas in the PYK2-deficient aorta, the reduced relaxation response was suppressed further to a level comparable to L-NAME–treated

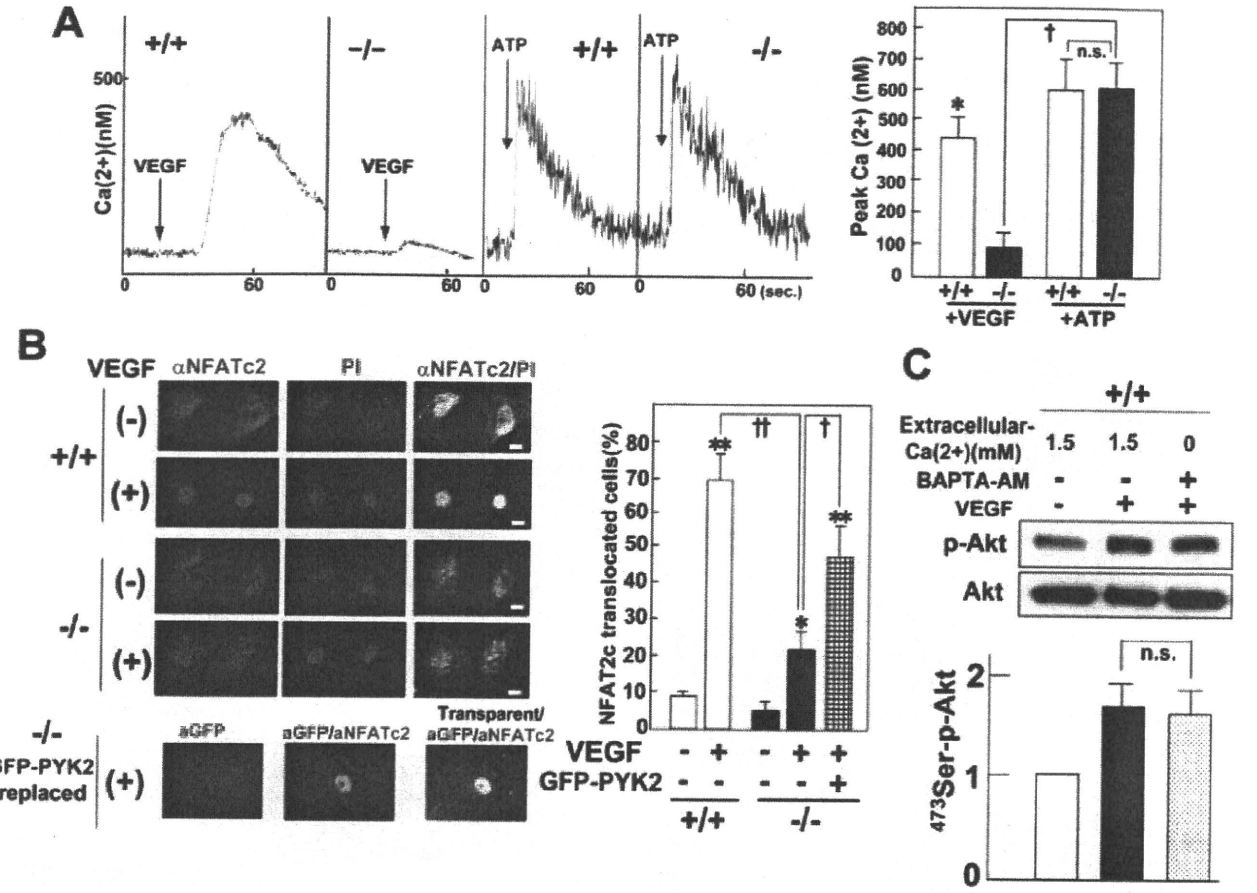

Figure 3. Impaired Ca^{2+} mobilization in PYK2-deficient mice. A, VEGF (100 ng/mL) - or ATP (1 mmol/L) -mediated cytoplasmic Ca^{2+} concentrations were measured in Fura-2–loaded ECs by a fluorescence microscope (n=12 each). †$P<0.001$, *$P<0.001$ vs VEGF-stimulated $PYK2^{-/-}$ cells. B, Top, ECs were fixed with 4% paraformaldehyde 30 minutes after VEGF stimulation, treated with 0.05% triton, and immunostained with anti-NFATc2 antibodies and propidium iodide (PI). Bottom, PYK2-deficient ECs were transfected with GFP-tagged PYK2 plasmid. Forty-eight hours after transfection, cells were stimulated with VEGF for 30 minutes and immunostained with anti-NFATc2 and anti-GFP antibodies. The number of cells in which NFATc2 was translocated to the nucleus was counted and shown relative to total plated cell numbers (n=4 in each experiment). *$P<0.05$, **$P<0.005$ vs nonstimulated control cells. †$P<0.05$, ††$P<0.01$. Scale bar=10 μm. C, After serum starvation (0.5% FBS) for 16 hours, cells were preincubated with BAPTA-AM (5 μmol/L) in the Ca^{2+}-free medium for 45 minutes and subsequently stimulated by VEGF for 5 minutes. Lysates were subject to immunoblot by antibodies against Akt and ^{473}Ser-phosphorylated Akt.

wild-type aorta (from 32±8 to 18±3%; $P<0.005$; n=4). These findings indicate that Ach-mediated vasorelaxation depends mainly on NO production, in which an involvement of PYK2-mediated NO signaling was estimated to be ≈64% [(59−32/59−17)×100] of the total NO-mediated vasodilation activated downstream of Ach. NO donor (nitroprusside) –induced vasorelaxation of the aorta was similar in both groups (82±4 versus 83±4%; n=5), suggesting that NO-mediated signal transduction for vasodilatation is not impaired in the PYK2-deficient aorta (Figure 4C).

NO-mediated vasodilatation requires cGMP as a second messenger. We therefore measured the amount of cGMP in the aorta. Basal cGMP production in the $PYK2^{-/-}$ mice was 41% lower than that in the wild-type mice. Ach increased aortic cGMP production 4.8-fold in the wild-type mice, whereas the increase in the $PYK2^{-/-}$ mice was 2.0-fold, significantly ($P<0.01$) lower than in the wild-type mice (Figure 4D).

Decrease in Neovessel Formation by PYK2 Deficiency

Angiogenesis in the ischemic tissue requires eNOS activation.[17] We analyzed the blood flow recovery and neovessel formation after hind-limb ischemia. The ratio of blood flow recovery assessed by laser Doppler imaging was significantly lower in the $PYK2^{-/-}$ mice than in the wild-type mice (50% versus 76% recovery at 3 weeks after ischemia; $P<0.01$; Figure 5A). Oral administration of L-NAME (3 mmol/L in drinking water) significantly reduced the recovery ratio in the wild-type (from 76% to 62%; $P<0.05$) and $PYK2^{-/-}$ (from 50% to 37%; $P<0.05$) mice (Figure 5A). Considering that the recovery ratio of the L-NAME–treated wild-type mice (62%) is close to that of the $PYK2^{-/-}$ mice (50%), the blood flow recovery after hind-limb ischemia is considered to be regulated mainly by PYK2-mediated NO signaling. We also counted the number of $CD31^+$ vessels in the ischemic muscle. There was no significant difference in the basal vessel